Differential Protection Malfunction due to Transformer Inrush-Induced Harmonics

A Hardware-in-the-Loop Simulation Case Study Using RTDS to Optimize Relay Configuration

Thesis Report

Author:
Mischa Rozema

Supervisor:	Prof. Marjan Popov,	TU Delft
Thesis Committee:	Dr. Mohamad Ghaffarian Niasar,	TU Delft
	Ir. Niels De Winter,	TenneT

August 11, 2025

TU Delft Delft University of Technology

TenneT

Foreword

This thesis was written as part of my Master's program in Electrical Engineering at TUDelft. The project was conducted as a collaboration between TenneT and TUDelft.

Throughout this project, I was particularly motivated by the challenge of balancing theoretical understanding with practical implementation. The work presented here reflects both my academic interests and the hands-on experience I gained during my thesis and throughout my educational career.

I hope this thesis contributes meaningfully to the ongoing work of TenneT and helps improve the security of the Dutch electrical supply.

1 Abstract

On 19 December 2021, a single-line fault during energisation occurred in a grid segment in the Netherlands, which was caused by a defective earther fault that failed to disengage. During the fault, the implemented differential protection scheme failed to operate as intended, resulting in a delayed response of 189 ms.

This thesis aims to clarify the root cause of the malfunction and prevent any similar problems in the future. While the cause of the electrical fault was quickly identified, the reason behind the relay malfunction remained unclear.

The affected network segment was modelled using the Real Time Digital Simulator (RTDS), a tool capable of accurately replicating fault conditions. The RTDS surpasses conventionally used fault playback tools, as it can simulate a wide range of dynamic system behaviours. The protection relay was connected in a Hardware-in-the-Loop (HIL) setup to test its real-time response.

Testing with the RTDS revealed that tuning specific relay settings can effectively prevent the malfunction during future fault events. Nowadays, modern numerical relays offer a wide range of powerful protection functions. The intended behaviour of these functions, along with their impact on the relay's response, must be carefully considered to prevent malfunctions.

2 Acknowledgements

Firstly, I would like to thank Marjan Popov for granting me the opportunity to work on this project under his care. Furthermore, he had shown great character during meetings and when tasked with difficulties throughout the project.

The effort, support and advice on the technical aspects of the project received from Jeffrey van Hemert and Leo Ginder deserve to be mentioned here. There were many instances where problems encountered in the project, such as wrong arrangements within the test setup, were easily fixed with their expertise. They also provided feedback on the writing, specifically the technical aspects of the network and relays.

Niels De Winter provided valuable support to the project, and his efforts must be acknowledged. The project would not be finished without his necessary interventions and check-up moments. His strict and direct work ethic might invoke frustrations. However, he gave me the impression that he genuinely cares about efficient work, and TenneT should be lucky to have him on board.

Completing a project of this magnitude can sometimes feel lonely and monotonous. Fortunately, I had the pleasure of being accompanied by a great friend. Noah Legerstee, your company was truly appreciated throughout my thesis journey. I wish you the best of luck with your upcoming studies. I only hope you get better at board games in the future.

I want to express my gratitude to the individuals who took the time to peer review my work. Marnix Massar and Richard Rozema provided valuable suggestions to improve the flow and readability of the writing. The quality of the thesis would have been significantly lower without their input.

I would like to sincerely acknowledge the support of my parents throughout my time at TU Delft. Thanks to them, I have had the privilege of embarking on my academic journey. Moreover, I was fortunate to live at home for most of my studies, which made this experience much more manageable. Thank you, it would not have been possible without you.

Finally, I would like to thank my girlfriend, Suzanne Alderliefste. I know I have not always been the easiest person to be around, nor the best roommate during my thesis work, and for that I apologise. Your unwavering support has been a constant source of motivation, helping me push through to the ever-shifting finish line. I am genuinely grateful, and I look forward to spending much more time together now that my studies are coming to an end.

Contents

3 Introduction

3.1 Overview

According to TenneT, the Dutch Transmission System Operator (TSO), the availability of the electricity supply is higher than 99.99%. Nevertheless, faults are inevitable when operating a complex system with dynamic components.

Generally, several methods are used to achieve a high level of grid availability. One such method is through the use of numerous redundant protection mechanisms that reduce the impact and severity of network faults by quickly isolating fault areas. However, an important question is what happens when these mechanisms fail.

Protection devices can experience several types of malfunctions. For example, a relay can trip unnecessarily without a genuine electrical fault or overload, which is known as nuisance tripping. In addition, extended usage can deteriorate the relay, causing it to fail altogether. Another malfunction is when the relay does not react to a fault when it was expected to do so. Figure 1 displays a confusion matrix of the malfunctions, illustrating the relay reactions in relation to the network conditions.

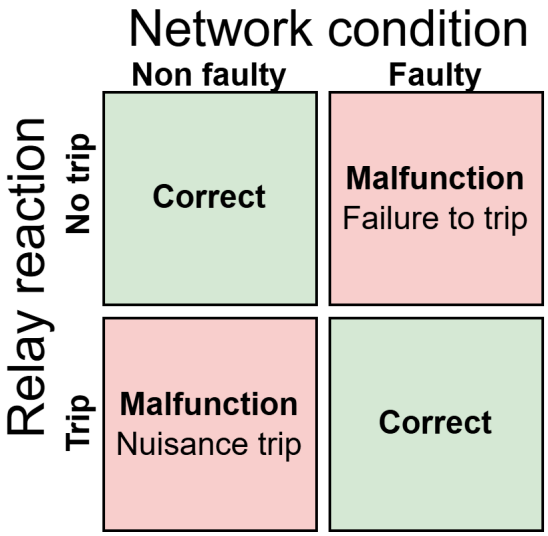

Figure 1: Confusion matrix of types of relay malfunctions.

Among these malfunctions, the 'no trip under faulty conditions' reaction is particularly relevant, as it sets the stage for the discussion in the case study. This type of malfunction occurred in a differential protection scheme within the Dutch grid in 2019. The origin of the fault was obvious, a mechanical failure of an earther. However, the sequence of events that led to the relay to malfunction has yet to be explained.

This research aims to expose this sequence of events by investigating the underlying phenomena and simulating the fault in the case study using a Real Time Digital Simulator (RTDS), a powerful computer for the simulation of electrical networks. Afterwards, recommendations will be made to prevent future malfunctions. Furthermore, the protection scheme will also be thoroughly tested with other fault circumstances to verify the robustness of the recommendations.

3.2 Problem definition

The context of the case study is necessary to accurately define the problem. The protected network section connects two substations, Eemshaven Midden 110 kV (EHM110) and Robbenplaat 220 kV (RBB220). Its primary components are a transformer and a cable, which are enclosed and protected by two pairs of differential relays. The arrangement of components can be seen in the single line diagram of Figure 2.

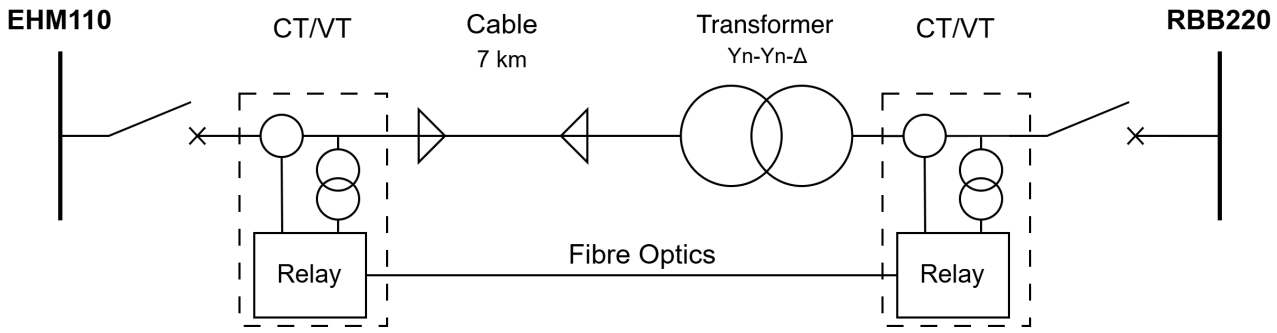

Figure 2: Single line diagram of the protected region.

The network components of the protected region impact the effectiveness of the differential protection scheme. Transformers and cables both draw higher magnitudes of current than usual when they are energised. Additionally, energisation is associated with additional unintended or adverse effects, such as signal distortion causing harmonic content and DC components. These effects make the measurement equipment susceptible to saturation, leading to further problems.

These issues are usually premeditated and resolved by the installed relays. The relay type used in this network segment is the Siprotec 4 7SD5, a commonly used type of differential protection device in the Netherlands. Currently, they are gradually being replaced with newer versions. However, it would be capital-intensive to change the remaining operational relays when it is not necessary, as the relays' functionalities are flexible and robust enough to keep up with modern relays.

It is beneficial to find a method to prevent the malfunction of the currently installed protection hardware. This might be achieved by tuning the parameters of the relay found in its configuration. The configuration is a list of customizable settings that is implemented in the relay and consists of hundreds of parameters that influence the behaviour of the relay and its reactions to the electrical faults. As a result, there might be a combination of settings that is insensitive to the original malfunction.

The main problem definition can be defined as: 'How to prevent future malfunctions of the differential and other protection schemes due to transformer inrush-induced harmonic content by changing the Siprotec 4 7SD5 relay's configuration?'

3.3 Project objectives

The main purpose of this report is to provide accurate recommendations for preventing delayed response times caused by transformer inrush-induced harmonic content. For this purpose, a case study using the RTDS is performed. This entire process can be described using the following bullet points:

- Accurately reproduce the faulty operation that occurred in the electrical grid.
- Scientifically explain the phenomenon behind the malfunction.
- Predict and describe the reaction of the protection mechanism with other fault configurations, such as:
  - Different fault locations within the protected region.
  - Other types of faults (e.g. phase-to-phase, three-phase and single-phase faults)
  - Different network segment conditions, namely, pre-energisation, half-energised, and steady state.
- Propose recommendations for proper relay configurations to prevent further malfunctions.

3.4 Thesis layout

This report will outline the process of optimising the relay configuration from the beginning to the end. The background of differential protection will be given, the case study will be fully explored, an explanation of the Hardware-in-the-Loop (HIL) simulation will be covered, and an analysis of the simulation's result will be given. A detailed overview of the thesis layout is presented in the upcoming paragraphs.

First, Chapter 4 will dive into the case study. An overview of the affected electrical grid segment will be given, including the relevant grid components. The current waveforms, which were measured during the fault, will be investigated to gather practical parameters for constructing and tuning the simulation. This information will be used to build the HIL simulation.

Next, Chapter 5 provides a brief overview of differential protection. It reports the basic principles and underlying phenomena that generate false differential currents, making the protection mechanisms complex. Protection engineers have proposed several methods to mitigate these phenomena, which will also be reviewed in this section.

The implementation of the HIL simulation will be discussed in Chapter 6. The applied model takes into account all significant design details. The required general layout and features of the model will be addressed. Then, the components presented in the general layout will be further developed in the subsequent sections. The thought process behind the selection of values will be explained for each parameter.

Chapter 7 discusses the testing procedure that was followed throughout the testing phase. It describes a priority list, in which tests are to be executed sequentially. The list begins with the basic setup, gradually expanding to include, firstly, the relay parameters, then fault circumstances such as scenarios, locations, and conditions, and finally other relevant relay models. This section explains why specific configurations are considered and why others are excluded from this report.

Chapter 8 will provide an analysis of the results of the testing procedures. It will highlight the origin of the erroneous behaviour and which relay parameters are most susceptible to inducing malfunction. The same principle will also be applied to different configurations and relays as described in the 'Test Procedure and Methodology' chapter.

Ultimately, Chapter 9 will provide clear recommendations for the relay configuration to prevent faulty operations. Moreover, more general recommendations will be made for all similar situations. Chapter 10 will cover areas not addressed by this project, and thus remain open for future work.

4 Fault Analysis

A clear understanding of the case study is crucial before recreation and simulation are possible. This chapter is dedicated to this purpose. Detailed insight into the relevant background information about the faults and the protected region that was supposed to operate will be provided.

The analysis is divided into three sections. Section 4.1 describes the fault progression and associated consequences, providing an overview of the case study. Next, Section 4.2 summarises the relevant network components present in the protected region and their relevant characteristics. Finally, Section 4.3 describes the current waveforms of the fault event and the prominent characteristics revealed within.

4.1 Fault progression and impact

The specific grid segment where the fault occurred is a crucial connection to various major providers and pieces of transmission equipment, including a range of traditional fossil fuel generators, wind farms, solar panel fields, and the NorNed HVDC connection, which has a rated capacity of 700 MW. A disruption could result in a significant power loss. The information presented in this section is based on internal outage reports documented by TenneT [1, 2].

During system restoration, a Single-phase to Ground (LG) fault occurred within a transformer bay of the RBB220 substation. An earthing switch on the transformer HV side suffered a mechanical defect, which prevented the switch from disconnecting all three poles when requested; the national control room did not receive a failure-to-operate alarm. The error was not registered. A short circuit current immediately started to flow when the circuit breakers were closed.

Unfortunately, the protection scheme protecting the bay did not operate as expected. The grid segment includes two types of protection: differential protection and distance protection. As the fault occurred within the protected region, the differential protection was expected to detect the large differential current and open the circuit breakers on time. However, this reaction was unreasonably delayed.

The relay's response time to the fault was 189 ms; a typical reaction of the integrated differential protection would be 35-45 ms or even faster [3]. This excessive delay resulted in backup protection mechanisms disconnecting other parts of the grid to isolate and clear the fault, causing an unnecessary power outage accounting for approximately 2.3 GW. However, the original cause of the delayed reaction remained unknown.

4.2 Description of the protected region

The components that make up the electrical system have a similar defining impact on providing the necessary information needed for this project as the events surrounding the fault occurrence. Therefore, this section will establish the required electrical network layout that is relevant to understanding the case study and its results.

The protected region in question is composed of various grid components. The primary equipment comprises 2 circuit breakers, a 7 km long cable, a 370 MVA-rated coupling transformer, and the necessary earthing switches. The included secondary equipment is related to differential and distance protection, which includes combined instrumental transformers, protection relays, and transmission equipment such as fibre-optic converters. Figure 3 shows an overview of the protected region and its installed protection mechanisms.

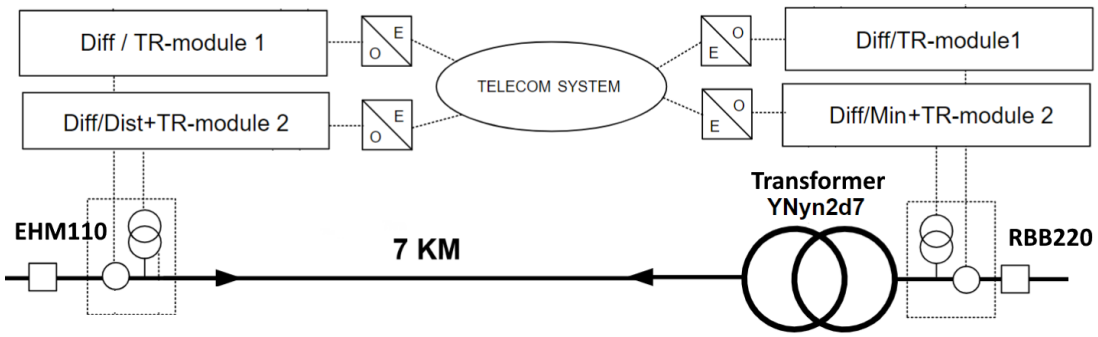

Figure 3: Overview of the protected region and its installed protection mechanisms

The 7 km bundle of cables [4] has two cables per phase - a double circuit. It is a 1-core radial and longitudinal water-blocking power cable rated 132 kV. It can withstand short-circuit currents of up to 332,3 kA for half a second. The grounding mantels used for the cables are cross-bounded. The outer diameter is approximately 107,3 mm.

The three-phase transformer (YNyn2d7) [5] couples the 110 kV Low-Voltage (LV) circuitry to the 220 kV High-Voltage (HV) side. The core consists of a five-limbed design. The transformer is equipped with an on-load tap-changer, allowing the grid operators to adjust the HV side level $\pm$ 15% of U_N. However, the extremities are seldom reached; at most, only three taps are used for grid stabilisation. The primary and secondary windings are connected in a star configuration, and both neutral points are grounded.

Additionally, the transformer contains a tertiary delta-connected winding, which is unused. The open-circuit tertiary delta-connected winding has a positive effect on the zero-sequence current, as it permits the circulation of zero-sequence currents through it. Zero-sequence harmonic components (i.e., the 3rd, 6th, 9th and so on) are trapped within this winding, providing passive interference filtering. Moreover, any large voltage unbalances caused by short-circuits are compensated as large currents are trapped inside the tertiary winding. Therefore, possible large overcurrents are limited, thereby reducing the transformer's likelihood of overheating during faulty conditions. The connection diagram of the transformer can be seen in Figure 4.

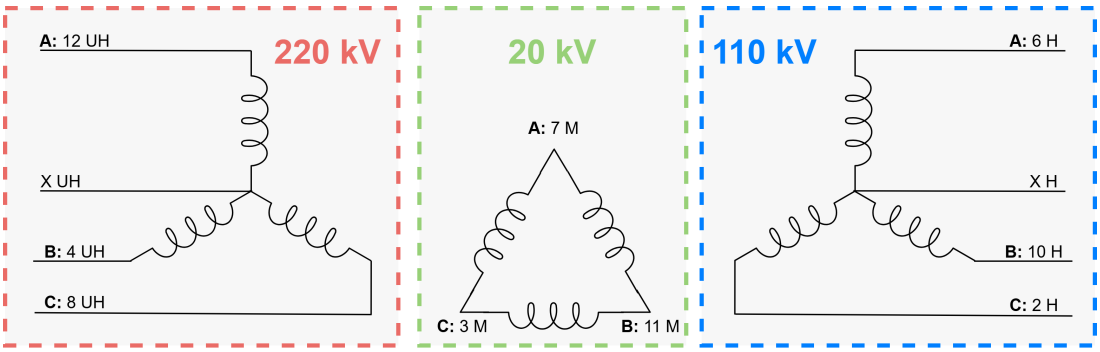

Figure 4: Connection diagram of the inner windings of the transformer (YNyn2d7).

Here, a few observations are of interest. Firstly, two-phase notations are used, namely a letter and a numerical representation (e.g. A and 12 UH). It is a common practice for TenneT to use a numerical notation. However, as the relays correct the phase, it does not affect the case study. The letter notation suffices and will be used throughout this paper. Additionally, the acronyms Ultra-High-Voltage (UHV) for 220 kV, High-Voltage (HV), 110 kV and Medium-Voltage (MV) for 20 kV used by TenneT are not used. Instead, 220 kV is referenced as HV and 110 kV as LV. The 20 kV is not relevant and is ignored throughout the thesis.

Two sets of instrumentation combi-transformers measure voltages and currents. However, only current measurements are of interest in differential protection. From now on, only the Current Transformers (CTs) will be mentioned. A set of CTs [6] is housed after the cable termination on the LV side. It has a conversion rate of 1.600-3.200/1, which means that the ratio can be configured. The transformer ratio of 3200 is used. Its accuracy class is 5PR60. The HV side CTs [7] has the same accuracy class. However, the HV side has a conversion rate of 2500/1. The numerical nature of the relays trivially ensures that the mismatched conversion rates do not cause any issues.

A pair of Siprotec 4 7SD5 units is connected to each set of CTs. The first unit functions only as differential protection, while the second unit provides both differential and distance protection. Due to the length of the cable, the respective units are connected via fibre-optic wires. Naturally, there are other outgoing connections, such as to supervisory technology, such as SCADA, and operational equipment, like the Circuit Breakers (CBs) enclosing the protected region.

Fibre optics carries the relay's output and input signals. However, the communication link's medium spanning the length of the cable is electrical; the signal medium needs to be converted from fibre-optics to electrical, and back to fibre-optics after reaching the other side of the network segment. Devices called *G.703* perform this action in the network segment. The G.703s operate at a speed of 64 kbps. Regardless of the speed, the data transfer introduces time delays, and conversion could result in lost messages. The possible delays can be neglected in the present project as the physical circuit dimensions are small [8].

A summary of the relevant network components is shown in Table 1.

Component	Description	Quantity
Transformer	Three winding, 370 MVA, rated 220/110/20 kV, YNyn2d7.	1
Cable	7 km length, rated 110 kV.	2
CT	LV side 3200/1 and HV side 2500/1 winding ratios.	6
Relay	Siprotec 4 7SD5, two modules: 1) differential, 2) differential + distance.	4
Signal converter	Fibre optic to G.703 co-directional conversion, 64 kbs conversion rate.	4

Table 1: Summary of all relevant grid components in the protected region.

4.3 Distinctive characteristics of fault currents

To accurately reproduce the fault condition, it is essential to understand the current waveforms when examining an oscillographic representation, such as Figure 5.

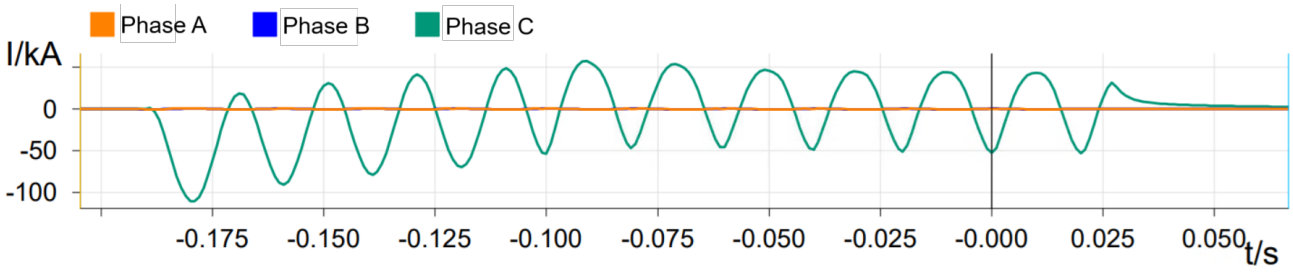

(a) All phases

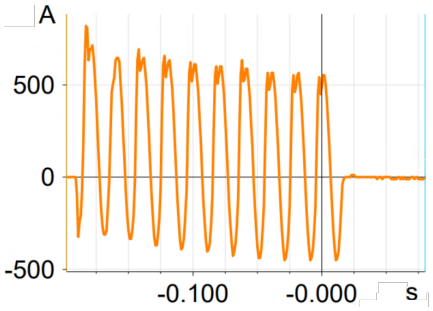

(b) Phase A (y-axis zoomed in)

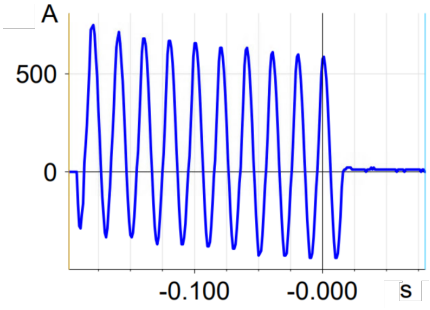

(c) Phase B (y-axis zoomed in)

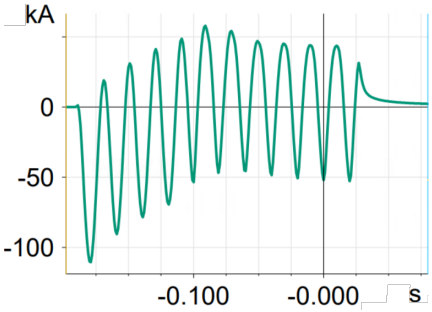

(d) Phase C

Figure 5: Currents of the three phases measured at the HV side during the fault event.

The graph shows a case of three current waveforms measured from the HV-side CTs, one plot per phase. The last plot (drawn in green) contains the faulted component. The vertical black line indicates the exact instant when the relay picked up the fault event. Three important sightings can be drawn from this Figure. Namely, an exponentially decaying *DC-offset* in the faulted phase, an imbalance in current indicating a significant *ground current*, and distortion caused by the *second harmonic*. These three phenomena are explored in the following sections.

4.3.1 DC-offset

A significant DC fault current can be seen in the faulted phase. The DC current can also be seen in the other phases with a lower amplitude. The DC component is caused by the energisation of the inductive windings of

the transformer after closing the circuit breakers. The equation for current in an inductor is given in Equation 1.

$$i(t) = \frac{1}{L} \int_{t_0}^{t} v(t)dt + i_0 \tag{1}$$

Herein, $i(t)$ is the instantaneous current $[A]$, L is the inductance $[H]$, v(t) is the instantaneous voltage $[V]$, t_0 is the time of energization and i_0 is the initial current $[A]$, which is zero before closing the circuit breaker. It is evident from the equation that the moment of activation is crucial to the height of the DC component.

The largest DC-current is drawn when an inductor is energised at voltage zero. The current is correlated with the integral of the excitation voltage, or in other words, the area under the voltage waveform.

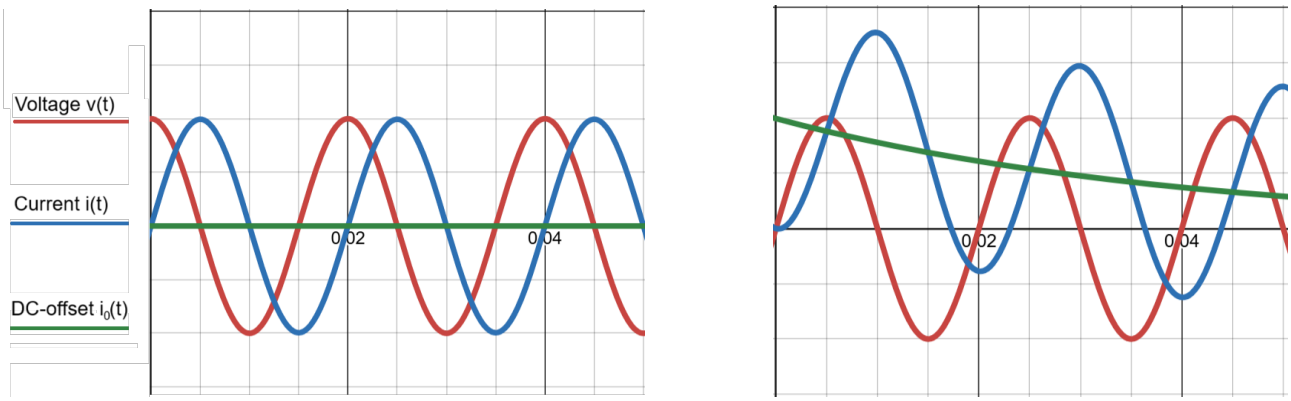

(a) Closing CB during voltage maximal amplitude.

(b) Closing CB during voltage zero crossing.

Figure 6: Demonstration of the impact that CB's closing timing has on the DC-offset.

The resistances of the circuit dissipate the DC component. The largest and most influential resistance prominently defines the speed of this process. A formula for an ordinary exponentially decaying DC-component is given in Equation 2.

$$i_{DC}(t) = \begin{cases} 0 & \text{for } t \in (-\infty, 0) \\ I_0 e^{\frac{-t}{\tau}} & \text{for } t \in [0, \infty) \end{cases} \quad \text{where } \tau = \frac{L}{R} \tag{2}$$

In this formula, i_{DC} is the instantaneous DC current component, I_0 is the component's magnitude $[A]$, and τ is the inductive time constant. This constant is defined as the time at which roughly 63.2% of the final value is reached (the constant can be calculated from $1 - e^{-1}$). A higher time constant means the component dissipates more slowly.

The DC component of a fault current negatively influences the response of a differential protection scheme, as it can cause CT saturation, generate harmonic content, and distort the measured values. Additionally, the DC component could also influence the results of the relay's measuring and sampling techniques. Therefore, incorporating the DC component into the test setup is essential to represent the fault accurately.

4.3.2 Ground fault current

A grounded fault typically results in a substantial flow of ground fault current [9]. This was also the case for this configuration. It can be seen more clearly by summing up each phase to create the single-phase fault current as $I_A + I_B + I_C = 3I0$ as shown in Figure 7.

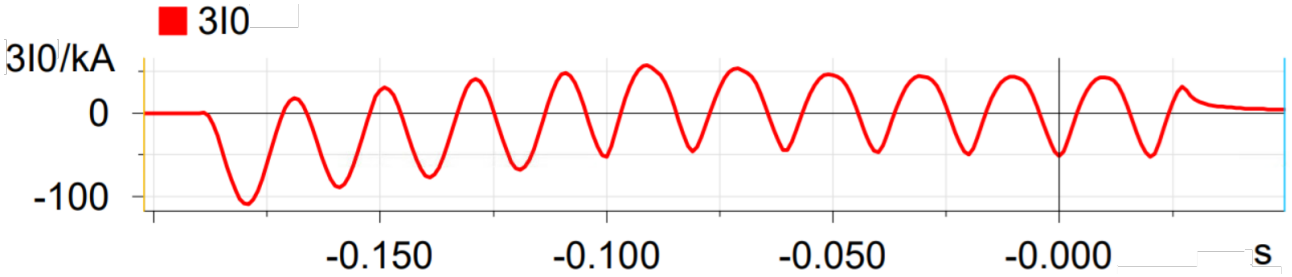

Figure 7: Waveform of ground current.

It can be seen that the ground fault current is mostly the same as the current in the faulty phase. The non-faulty phases have almost no effect on the magnitude of the ground current. Up to about 100 kA, an instantaneous current flows through the ground.

The magnitude of the ground fault current compared to the phases of the power system is a significant factor in verifying the correct operations of an equivalent system model. The ground fault current characteristic must be considered when designing the test setup.

4.3.3 Presence of the second harmonic

All phases are subjected to harmonic distortions, and specifically, the 2nd harmonic is prevalent. [10]. Three harmonic features can be seen: a 'lob-sided' current shape, a dip when the current reaches its peak, and a significantly steeper angle at the sloped parts than that of a normal sinusoidal waveform.

A graphical representation is used to explain these harmonic features. Figures 8a and 8b shows two signals with a second harmonic superimposed; the former with a 90-degree phase-shifted 2nd harmonic, and the latter with a 180-degree phase shift.

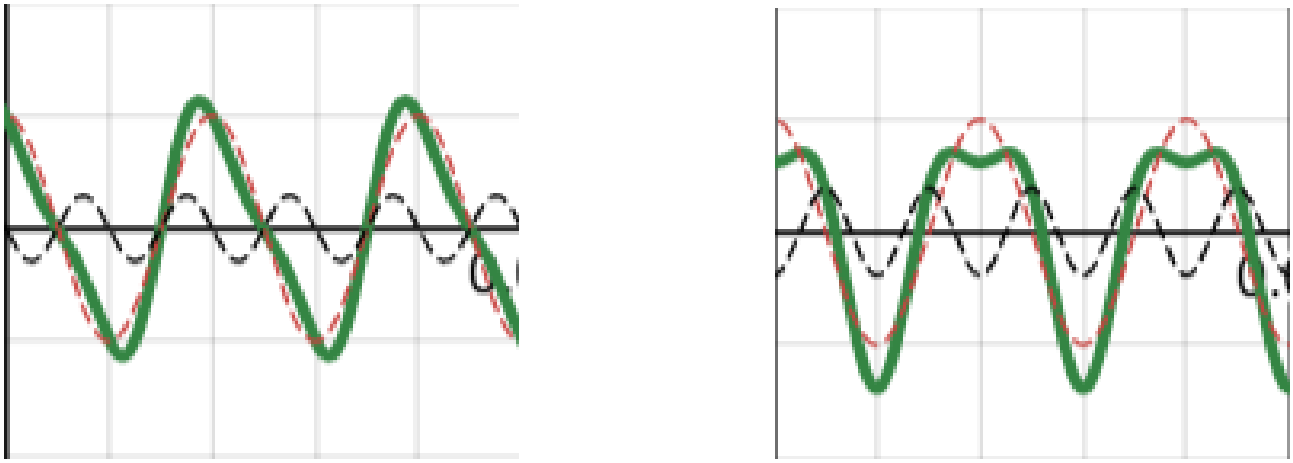

(a) 90 degree phase shifted.

(b) 180 degree phase shifted.

Figure 8: A 50 Hz signal superimposed with the second harmonic.

Several relay functionalities within differential protection operate based on the magnitude of harmonic content measured inside fault currents. The second harmonic is often used to restrain relay tripping. Therefore, it is a crucial fault characteristic that should be incorporated into the equivalent system model.

In conclusion, three fault characteristics are extracted from the measured current waveforms, namely, the DC-component, the ground fault current and the second harmonic content. These characteristics have the potential to influence the behaviour of the installed protection mechanisms and should be considered when designing a model that reproduces the faults.

5 Overview of Differential Protection

Differential protection is a frequently used type of protection in three-phase electrical power systems. It is used for various grid components, including generators, feeders, large industrial loads, bus bars, and transformers. The simple operating principle allows for fast implementation and offers high sensitivity. However, under specific circumstances, non-faulty differential currents can cause the protection scheme to trip unnecessarily. Nevertheless, these phenomena are expected and mitigated using a variety of methods.

The first section examines the concept of differential protection, including its benefits and drawbacks. Later, section 5.2 explores natural processes that can induce non-faulty differential currents. Section 5.3 describes in-depth methods on how to mitigate malfunction due to false differential currents. Finally, Section 5.4 applies the discussed theory to the Siemens Siprotec 4 7SD5 relay, which is used in this study.

5.1 Differential protection

The operating principle of the differential protection follows a relatively simple concept [11]. It uses Kirchhoff's first Law, which states that the sum of all currents entering a grid node or segment should result in zero at all times. When a differential current is detected (i.e. the sum of currents does not equal 0), there is a fault within the protected region. The principle is shown in Figure 9.

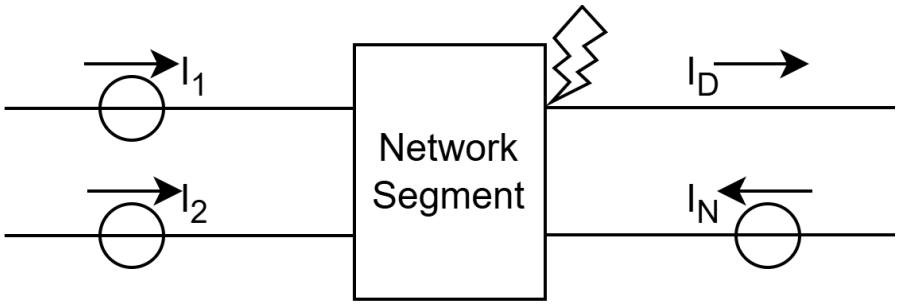

Figure 9: Showcase of the principle of differential protection.

The differential current is calculated as $I_D = I_1 + I_2 + ... + I_N$ for N current paths entering a network segment. This project's case study focuses on the case of N = 2.

The differential protection principle has three key benefits compared to other types of protection. Firstly, the protection scheme offers a high sensitivity to internal faults. Due to the comparison of entering and leaving current, even minor discrepancies can be detected. Secondly, the high sensitivity leads to fast fault isolation and clearance. The potential damage to protected grid components is limited, and the reliability is increased. Finally, differential protection has clearly defined zones of protection. Under faulty conditions, unnecessary outages are prevented because only components within the affected zone are disconnected.

There are various classifications of differential protection. Each operates on different triggers and principles, such as current, voltage balance, and biased percentage differential relay. Moreover, the implementation can differ between electromechanical, digital, and numerical relays. This project focuses on the latest generation of *numerical current differential relays.*

5.2 Non-faulty differential currents

Several phenomena complicate the simple principle of differential protection. There are regularly occurring apparent differential currents due to different reasons, such as energisation or sudden topology changes. Relevant sources of false differential current are discussed in this section.

There are a few primary error factors relevant to this specific grid segment. First, lines and cables raise large capacitive inrush currents, the magnitude of which linearly depends on the length of the medium. Second, transformers experience high magnetising inrush currents only on the energised side due to the saturation of the iron core. Finally, transformer characteristics such as winding connections, tap changers, and grounding can influence the calculation of the differential current.

Furthermore, the measurement of analogue signals is prone to inaccuracies; this also applies to the instrument combi-transformers and relays. For example, the digital-analogue converters cause sampling errors such as quantisation errors. Moreover, the response characteristics of a CT, such as saturation and accuracy limiting factors, impede high fidelity. Transmission errors, such as signal jitter and time delay, also impact the measurement error.

5.2.1 Transformer inrush magnetising currents

Energising a transformer can create a large magnetising inrush current that could cause malfunction of a differential relay [12, 13]. This is because the transformer's energisation can cause its iron core to saturate. The core magnetic flux density B $[T]$ influences the onset of saturation. Generally, the flux within the core is made up of three parts: steady-state flux, excitation flux, and remnant flux.

Magnetic flux in the transformer core

The core saturates when the flux density exceeds a threshold, called the B_{max} limit [13]. The flux inside is dependent on three components [14, 15]: The steady state flux Φ_S, which is created during normal operation; the excitation flux Φ_E, dependent on the voltage point of activation; and the remnant flux Φ_R, which remains in the core when the transformer is deenergized. The relation between magnetic flux and excitation voltage of the winding is given in Equation 3.

$$\Phi(t) = \frac{1}{N} \int E(t)dt \tag{3}$$

Φ is the created magnetic flux $[Wb]$, N is the number of winding turns [-] and E is the winding's excitation voltage $[V]$. Under normal operation, the flux will be shaped sinusoidally when the voltage is an ordinary sinusoidal wave.

For example, if the excitation voltage is given by $E(t) = V_m sin(\omega t + \alpha)$, then the steady-state flux is given by $\Phi_S(t) = -\frac{V_m}{\omega N} cos(\omega t + \alpha) + c$. In these equations, V_m is the excitation voltage magnitude $[V]$, ω is the system frequency $[rad/s]$, α is a phase shift $[rad]$ relative to the positive zero crossing of the voltage signal, and c is a constant that will be defined later. This steady-state conversion example is visualised in Figure 10.

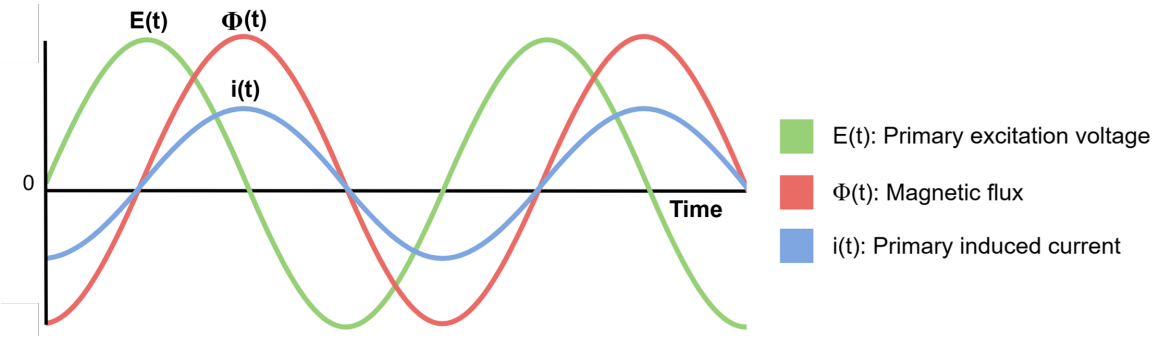

Figure 10: The magnetic flux in the core is defined as the integral of the excitation voltage. In steady-state conditions, this results in a phase shift of 90°

.

The moment of closing the CB is important for the flux density. An unfortunate timing, such as a zero crossing, will potentially double the invoked flux. The extra invoked flux is called *excitation flux* $[\Phi_E]$. The excitation flux is given as $\Phi_E = \frac{V_M}{\omega N} cos(\phi)$. This principle is illustrated in Figure 11. Here, in the grey area, is the flux in the first half cycle. All magnetic flux is positive in Figure 11a whilst the flux is centered arround the y-axis in Figure 11b.

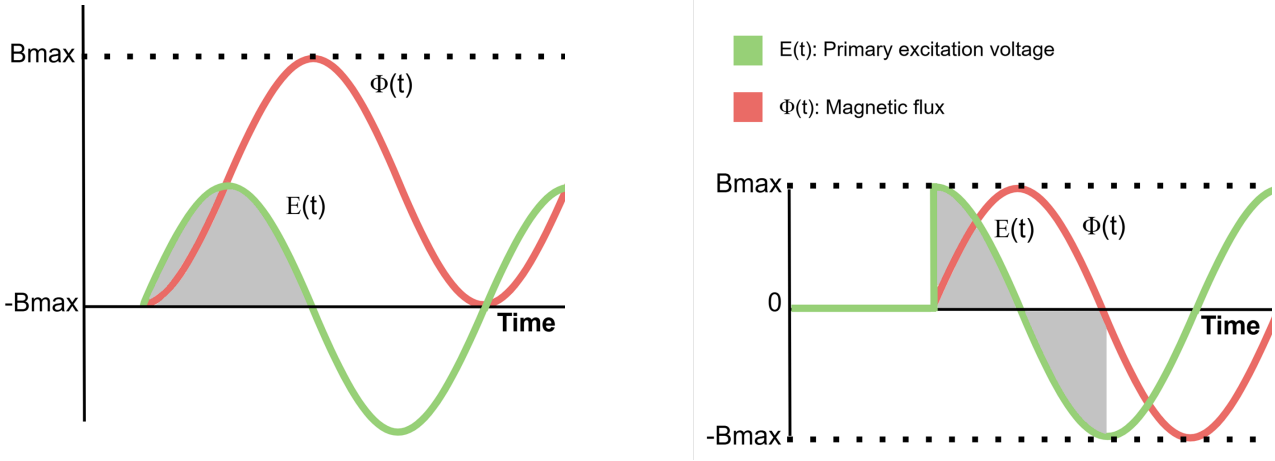

(a) Closing CB during voltage zero crossing.

(b) Closing CB during voltage maximal amplitude.

Figure 11: Illustration of the effect CB closing timing has on the induced excitation flux.

Another contributing factor to the total flux is *remnant flux* [Φ_R]. After aligning the magnetic moments of the transformer core and removing the external magnetic field, the magnetic moments do not necessarily return to their original orientation. A portion of the magnetic domains retains the alignment and requires extra effort to adjust. This process is also known as *hysterisis*. Essentially, remanent flux is caused by unfavourable de-energisation timings, and its magnitude is generally between 30% and 70% of $\pm\frac{V_m}{\omega N}$ [14].

Finally, when all the components are summed up [14], the equation for the total magnetic flux for a sinusoidal voltage signal is as in Equation 4. The maximal expected inrush current is approximately three to four times the rated current [3] of the circuitry.

$$\Phi = \Phi_S + \Phi_E + \Phi_R = -\frac{V_m}{\omega N} cos(\omega t + \alpha) + \frac{V_M}{\omega N} cos(\phi) + \Phi_R \tag{4}$$

From this equation, two crucial details can be concluded. First, the moment the CBs are closed has a significant effect on the magnitude of the inrush current. Secondly, the instance the transformer is deenergised influences the magnitude of the inrush current; the remanent flux needs to be controlled and monitored. To conclude this section, precise CB closing and remanent flux monitoring must be included when modelling the test system.

5.2.2 Cable capacitive inrush current

A capacitive inrush current will be generated when energising a cable or line. Equation 5 can be used to calculate the magnitude of the capacitive inrush current.

$$I_C = 3,63 \cdot 10^{-6} \cdot U_N \cdot f_N \cdot C'_B \cdot l \tag{5}$$

In this equation, I_C is the expected capacitive inrush current [A], U_N is the nominal voltage level [kV], f_N is the nominal frequency [Hz], C'_B is the cable's per unit length capacitance [nF/km], and l is the cable's length [km]. After calculating, this turns out to be approximately 43A. the calculated amount times three three times should be taken into account when designing the protection scheme [3].

The calculated cable inrush capacitive current is one order of magnitude lower than the expected transformer inrush current. For that reason, it will be neglected during the analysis as it does not have a significant impact on protection devices compared to other sources.

5.2.3 Phase shift due to transformer winding connections

The type of transformer winding connections can cause a phase shift between the primary and secondary windings. Specifically, a transformer containing a star and delta connection will create a 30° phase shift. Historically, this was counteracted by including a delta connection in one of the CTs. However, a modern numerical relay is capable of correcting this misalignment by applying software solutions.

5.2.4 Transformer ratio

In a coupling transformer, an unbalanced number of turns between windings generates a differential current. This difference can be adjusted by correctly setting the winding ratio of the CTs. Luckily, the introduction of numerical relays made this issue trivial, as a software solution can correct the misalignment due to the transformer ratio.

A coupling transformer, such as the one described in this document, often includes a tap-changer. This enables grid operators to adjust the transformer's turn ratio dynamically. This can help to stabilise the voltage level and improve power delivery efficiency by maintaining a constant voltage level. However, a tap changer negatively influences the effectiveness of differential protection mechanisms, as the static conversion error caused by transformer ratios becomes time-varying.

The installed tapchanger allows operators to vary the primary voltage magnitude between 187 and 253 kV (i.e. $\pm 15\% U_N$). This significant variance could impose challenges when designing differential protection, as the implied current is also directly affected. However, the extremities of the tapchanger settings are rarely used and are mostly restricted to a maximum of three taps (i.e., the magnitude mainly shifts between 213 and 226 kV). The effects of the tapchanger can therefore be neglected in this case study.

In summary, the combined effects of the factors mentioned in this section cause a significant error in the differential current. Some error factors, such as the saturation of CTs, even depend on the magnitude of the flowing current. Therefore, a dynamic restraining limit is required for protection operations to prevent unnecessary tripping of the relays.

5.3 Techniques used to mitigate unintended tripping

The differential current caused by magnetising inrush current can cause relays to trip unintentionally. Distinguishing between actual and inrush differential current is not a trivial task. Luckily, several methods for preventing malfunction have been invented [11, 13, 16]. Relevant trip-restraint techniques for the case study are explored here.

5.3.1 Threshold restraining

A simple restraining method commonly implemented is trip restraint using a current threshold. The relay will not trip when the measured differential current is below a customizable threshold. This method is not sensitive to magnetising inrush current and rather counteracts static sources of differential currents, such as sampling errors or network losses.

5.3.2 Harmonic blocking

Calculating harmonic content is a more sophisticated method for detecting harmonic content. A key feature of magnetising inrush current is its distinct harmonic content; the 2nd, 3rd, and 5th harmonics are the most prominent. Decomposing a signal into its harmonic components using a variant of the Fourier transform and calculating the magnitude of each component can increase the sensitivity of differential protection schemes.

The generation of harmonic content is not limited to magnetising inrush current. Other effects, such as CT saturation, overexcitation, sympathetic inrush and non-linear fault resistance, also invoke significant harmonic components. In these cases, it is unclear if blocking the tripping reaction would necessarily be advisable. Therefore, the differential protection should not be immediately blocked when harmonic content is detected. Instead, a threshold should be used to determine the operation range. The expression for the N^{th} harmonic percentage based on the fundamental frequency is given by $I_{N,\%} = \frac{I_N}{I_1}$.

The value recommended by Siemens for the threshold of the expected, percentual 2nd harmonic content is 15%. The relay should give a trip command when this limit is exceeded. The concept of blocking tripping based on harmonic content is commonly referred to as *inrush restraint*.

There are scenarios in which inrush restraint does not operate as intended. For example, a non-linear fault resistance could generate sufficient harmonic content to cause the differential to block falsely. A standard option to prevent this is to calculate the maximal expected inrush current. If the differential current exceeds this expectation, the tripping operations will not be blocked.

5.3.3 Harmonic inrush crossblock

Situations may arise where one transformer leg is saturated, while the others are not [17]. This can create a phase with a differential current but insufficient harmonic content to trigger the restraint response, potentially causing the relay to trip unintentionally. A method to prevent this is to block the other phases if any harmonic inrush is detected. This is called *crossblock*.

There are several methods for applying crossblock [15]. *1-out-of-3* blocks all phases if a single phase passes the inrush restraint threshold. *2-out-of-3* follows the same principle, but operates if two phases exceed the limit. *Averaging* calculates the average harmonic content over all phases and only blocks when the average exceeds the inrush restraint threshold. Table 2 summarises the crossblock strategies for inrush restraint.

Table 2: Summary of a variety of crossblock strategies.

Crossblock method	**Description**
Per-phase	Only restrain the phase which exceeded the harmonic threshold. Essentially, crossblock is not enabled.
1-out-of-3	If the 2nd harmonic threshold is exceeded in at least one of the phases. All other phases will restrain from operating.
2-out-of-3	If the 2nd harmonic threshold is exceeded in at least two of the phases. All other phases will restrain from operating.
Averaging	The 2nd harmonic percentage is averaged over all phases. The relay will only restrain if the threshold is exceeded.

From this table, only two crossblock methods are relevant to this thesis. The implemented type of relay allows engineers to select between only two methods: per-phase and 1-out-of-3 (i.e. crossblock disabled and enabled). Therefore, the 1-out-of-3 method is implied when crossblock is referenced.

It is worth noting that the term "crossblock" is primarily used internally by Siemens. Most other vendors have a different name or lack a name for this functionality. Other naming conventions used are *Inrush Restraint Mode* and *Cross-Phase Blocking Mode*. In cases where no name is defined, crossblock is commonly implemented through a form of programmable logic present within the relay.

5.4 Implementation of differential protection using the Siprotec 4 7SD5

The Siemens Siprotec 4 7SD5 [3] is considered for this project, as this type of relay is commonly installed on the Dutch HV network. Coincidentally, it is also the relay model that is installed at the faulted network segment.

The relay can be broken down into several functions. Important functions in the case study are the differential protection based on current (the *I-DIFF> function*), the fast differential protection based on charge (the *I-DIFF>> function*), and the *2nd harmonic inrush restraint function*. Each functionality comprises several customizable settings that influence the tripping behaviour of the relay. To clarify their structure and establish consistent terminology, this section provides a detailed explanation of each relevant setting.

5.4.1 Differential current tripping settings: I-DIFF>

The I-DIFF> functionality implements the fundamental differential protection principle in Siemens relays. To prevent the false tripping of the relay, a dynamic tripping restraint is included by using *restraining current* [i_{res}].

Several configurable settings define the behaviour of the I-DIFF> function. Three are related to Accuracy Limit Factor (ALF) of a CT, namely Settings 0251, 0253 and 0254. Two additional relevant settings introduce a minimum value to the restraining current to address other possible measurement errors, with a varying magnitude depending on whether the system is in steady-state operation or undergoing energisation. These are Settings 1210 and 1213.

The restraining current acts as a dynamic threshold for the differential current. Both currents are calculated simultaneously, and the relay trips only if the differential current exceeds the restraining current. A fault is reproduced in a test environment to demonstrate this principle. The demonstration is shown in Figure 12.

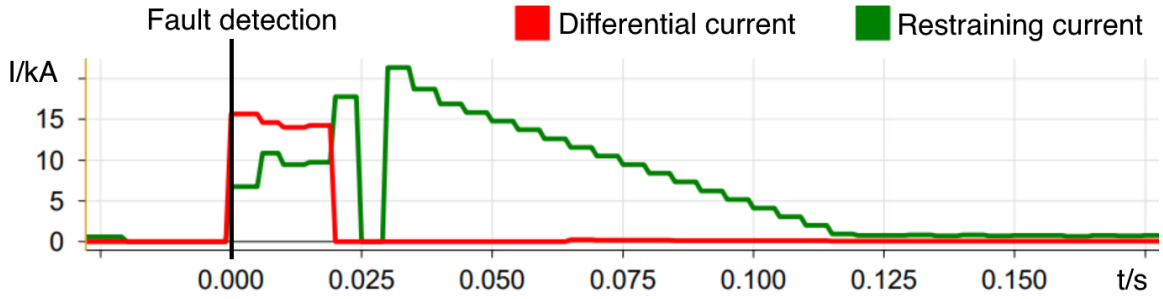

Figure 12: Demonstration of I-Diff> fault detection due to differential current exceeding restraining current.

At t = 0.000 s, the calculated differential current exceeds the restraining current. At this instance, the relay detects the fault and issues a close command towards the associated CB. The restraining current, which varies dynamically with several parameters, is computed using Equation 6.

$$i_{res} = \text{I-Diff} > + f_{sat,1} \cdot \epsilon_{ct,1} \cdot |i_1| + f_{sat,2} \cdot \epsilon_{ct,2} \cdot |i_2| + \Delta i_{sync} \tag{6}$$

Here, i_{res} is the restraining current, I-Diff> is the minimum threshold value defined by either Setting 1210 and 1213, f_{sat} is a factor that increases relative to the magnitude of all harmonic content, ϵ_{ct} are the error factors that increase relative to the magnitude of the measured current to account for CT measurement errors, $i_{1,2}$ are the measured currents and Δi_{sync} is an error margin to account for transmission delays.

A graph showcasing the tripping characteristic of the I-Diff> function can be seen in Figure 13a. Moreover, Figure 13b shows how the ALF parameters influence the error factor ϵ_{ct}. The selected parameter values are: Setting 0251 = 1.5 [-], Setting 0254 = 10%, Setting 0253 = 3%, Setting 1210 = $0.3 \cdot i_{\text{Rated}}[A]$, and Setting 1213 = $1.0 \cdot i_{\text{Rated}}[A]$.

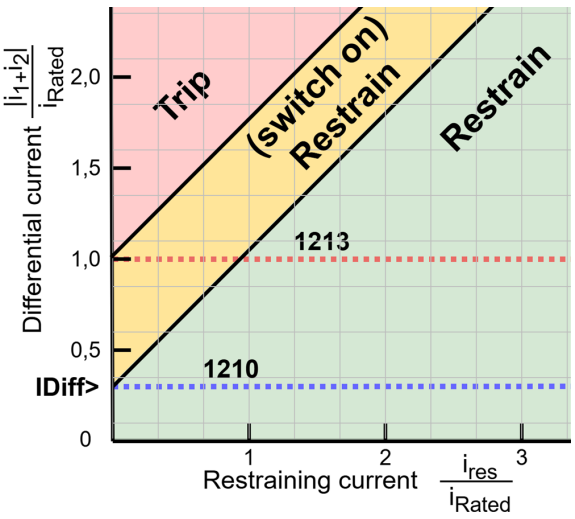

(a) I-Diff> tripping characteristic.

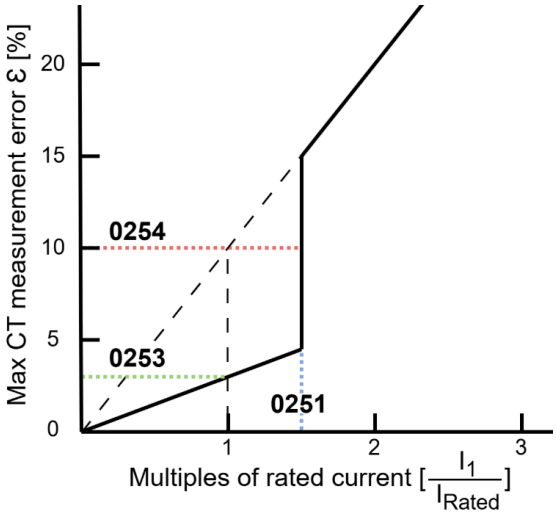

(b) Max CT error characterstic.

Figure 13: Graphical representation of the I-DIFF> functionality's characteristics.

In graph 13a, the differential current is plotted against the restraining current. It can be seen that the I-Diff> function becomes less sensitive during switch-on conditions. Additionally, the relay takes into account the increasing measurement errors from the CT.

5.4.2 Fast differential tripping reaction settings: I-DIFF>>

The I-DIFF>> function is similar to the I-DIFF> function. Instead of comparing currents, the fast differential functionality calculates charges. The I-DIFF>> function is intended to catch unmistakable high-magnitude faults. The charge calculation can be performed faster, but it is less accurate. The inaccuracy of the function is generally compensated for with a higher threshold value.

The behaviour of the I-DIFF>> function is defined by two parameters. The first, Setting 1233, represents the default pickup value. The second, Setting 1235, defines the pickup value applied during switch-on conditions, i.e., when the relay detects transformer and/or line energisation. The value for the switch-on conditions parameter must be configured higher to account for inrush characteristics.

The latter setting (switch on conditions) must have determined the I-DIFF>> threshold during the described fault, as the fault with the earther existed before the closure of the CBs.

5.4.3 Harmonic inrush restraint settings

The Siprotec 4 counteracts nuisance tripping due to magnetising inrush current by implementing *harmonic inrush restraint*. This function operates by first calculating the level of harmonic content. The relay will restrain from tripping if the level of harmonic content exceeds a configurable threshold. The harmonic restraint feature is customizable through four relevant parameters:

- **Setting 2301:** Inrush restraint.
- **Setting 2302:** 2nd harmonic in % of fundamental.
- **Setting 2305:** Maximum inrush peak-value.
- **Setting 2310:** Time for Crossblock with 2nd harmonic.

Setting 2301 specifies whether the harmonic inrush restraint feature is engaged. Setting 2302 determines the height of the 2nd harmonic threshold. Setting 2305 defines a threshold to which the restraint function is allowed to operate. The relay will always trip if this value is exceeded. Finally, Setting 2310 specifies the duration for which the relay applies cross-blocking when the harmonic threshold is surpassed.

Finally, a table summarising the relevant parameters and providing a clear overview is given in Table 3.

Table 3: Siprotec 4 7SD5 relevant configurable parameters.

No.	**Function**	**Settings**
0251	ALF	k_alf/k_alf nominal
0253	ALF	CT error in % at k_alf/k_alf nominal
0254	ALF	CT error in % at k_alf nominal
1210	I-DIFF >	I-DIFF >: Pickup value
1213	I-DIFF >	I-DIFF >: Value under switch on condition
1233	I-DIFF >>	I-DIFF >>: Pickup value
1235	I-DIFF >>	I-DIFF >>: Value under switch on condition
2301	Inrush restraint	Inrush Restraint
2302	Inrush restraint	2nd harmonic in % of fundamental
2305	Inrush restraint	Maximum inrush-peak value
2310	Inrush restraint	Time for Crossblock with 2nd harmonic

The overview of differential protection and the relevant Siprotec 4 settings described in the table are used to guide the design and construction of the equivalent system model and testing procedures. Several discussed settings will be experimented on to find a more optimal relay configuration to prevent the malfunction in the future.

6 Developing Testing System in RTDS

The case study is reconstructed using a real-time simulation to perform experiments to determine under which circumstances the malfunction occurs. The Siprotec 4 7SD5 is physically connected to the simulator to replicate the fault effectively. A simulation where hardware external to the simulator is physically connected is called a Hardware-in-the-Loop (HIL) simulation.

The constructed testing system is fully explored in this chapter. First, Section 6.1 describes the physical setup of all components of the HIL simulation. Then, Section 6.2 discusses the equivalent system model and its construction. Here, the model is broken down into smaller components and custom processes to improve the simulation are explained. Finally, Section 6.3 compares the replicated signal with the original fault to verify the ability of the developed test bed to reconstruct a near-real-time simulation.

6.1 Hardware-in-the-loop setup

The crucial component of the Real Time Digital Simulator (RTDS) infrastructure is the PB5 processor card. It is a previous generation of the RTDS's main processing hardware. Nonetheless, it is a powerful computational unit containing two processors operating at 1.7 GHz. Multiple PB5s can be linked inside a "rack" to combine their computational power. Furthermore, the processor cards are fully compatible with RTDS's end-of-the-line hardware solutions, such as the GPC cards and the NovaCor chassis.

On the back side, there are different digital fibre-optic connection ports, the purpose of which is to connect extension cards or other real-time processors. The RTDS can simulate complex networks using a typical timestep of 25-50μs. The simulator also uses smaller timesteps, called substeps, which enable the simulation of power electronic devices with switching frequencies in the 200 kHz range. The PB5 and the rack to which it is connected can be seen in Figures 14a and 14b, respectively.

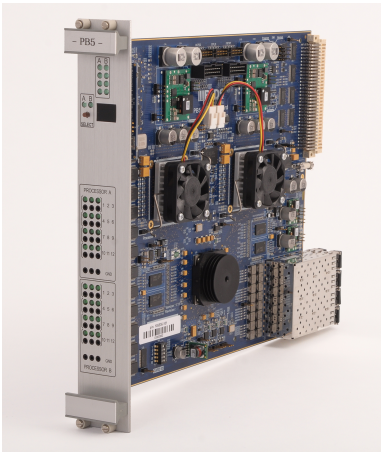

(a) PB5 processor card

(b) TU Delft's RTDS rack

Figure 14: Main processing hardware of the RTDS at TU Delft.

6.1.1 Hardware-in-the-loop components

Whilst the real-time simulation runs on PB5 cards, several extension cards have input and output interfaces. They allow the RTDS to communicate with real-life devices and perform HIL simulations. Optical cables connect the extension cards to the main chassis. Two such cards are of importance to the test setup, namely:

- The Gigabit-Transceiver Front Panel Interface (GTFPI).
- The Gigabit-Transceiver Analogue Output (GTAO).

First, the GTFPI card can handle incoming and outgoing digital signals. The card is directly connected to the front panel, which acts as an interface between simulated quantities and external hardware. The front panel provides 16 input and 16 output ports. The purpose of this card is to convey status updates to the relays and receive trip commands for the simulated CBs.

The GTAO card provides an analogue output from the simulation to external equipment. It has 16 outputs, which can be mapped to any signal within the simulation. The output range is between a maximum of ± 10 Vpeak. Herein, Signal mapping should be performed carefully, as supplying a too-small scaling factor will result in signal clipping. For example, if one output is configured to be 5V when the signal is 10kA, clipping will occur when the signal is above 20kA.

Unfortunately, the output of the GTAO cannot be connected directly to the input side of a relay. In real operation, a relay expects a higher input current. Thus, the signals require amplification from another electrical device, which is done by the Omicron CMS 156; it translates the voltage signal into a higher magnitude current waveform. The GTFPI, the GTAO and the Omicron amplification unit can be seen in Figures 15a to 15c.

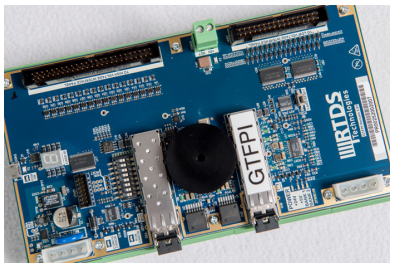

(a) Gigabit-Transceiver Front Panel Interface (GTFPI)

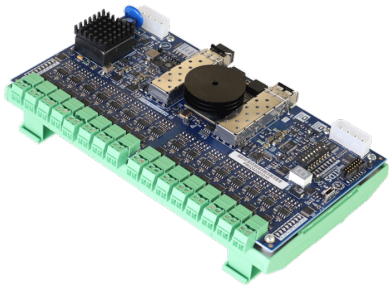

(b) Gigabit-Transceiver Analogue Output (GTAO)

(c) Omicron CMS 156

Figure 15: HIL components used to connect a relay to the RTDS.

The connections between the main simulation processor PB5, the GTAO, the GTFPI, the Omicron amplification units, and the relays are illustrated in Figure 16.

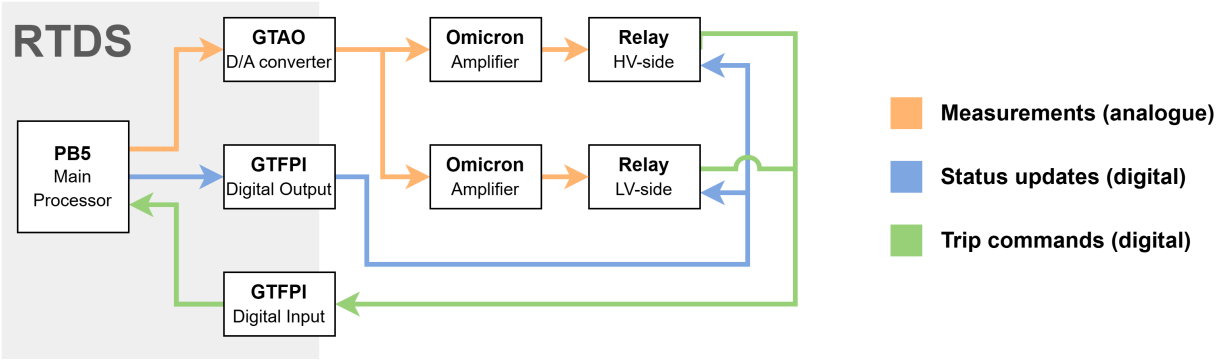

Figure 16: HIL simulation setup connection diagram showing how signals are transmitted between the components located in the HIL setup.

As shown in the diagram, the test setup differentiates between three types of communications: *analogue measurements*, *status updates*, and *trip commands*.

The analogue measurements are configured in a way that the current signals are calculated by the RTDS. The digital signals are converted into analogue by the Digital-to-Analogue (D/A) converter of the GTAO, which are then fed into the Omicron amplifier. The output is then connected to a relay. This process is performed twice, once for the HV side and once for the LV side.

The status updates are digital signals sent from RTDS to the relay regarding the state of the CBs (i.e., whether the CBs are open or closed). Six outputs are dedicated to this purpose; one for each phase of each relay. Finally, the trip commands are digital signals sent from the relays to the simulator. Using internal logic, a message is generated once the relay detects the fault. Again, six inputs are dedicated, one for each phase for each relay.

6.1.2 Amplification chain of the measurements

There are several amplification steps between the RTDS simulation software and the calculated primary current in the relay. The amplification chain must be properly calibrated to provide correct reproduction of the fault signal. The desired result scaling would be 1:1 (i.e., 1 kA in the simulation results corresponds to a measured 1 kA in the relay).

However, this is not as trivial as setting all amplification steps to 1. Several restrictions exist: firstly, the GTAO must not clip the signal; it must be capable of translating at least 100kA on the HV side and 200kA on the LV side. Secondly, the Omicron amplification is limited to the pre-set value of 5/1 [A/V]. Finally, each step must have sufficient bandwidth to prevent losing the low-amplitude signals within the noise.

A fitting solution for the HV-side and the LV-side amplification chain can be found in Figures 17a and 17b, respectively.

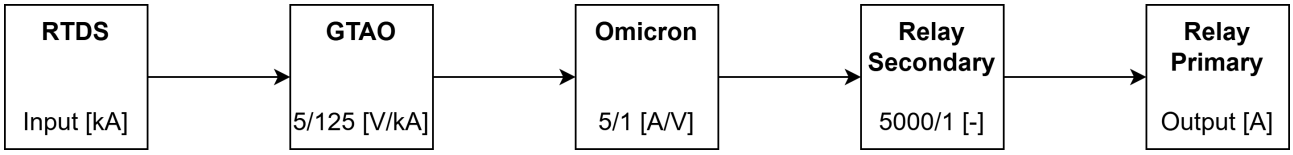

(a) HV-Side

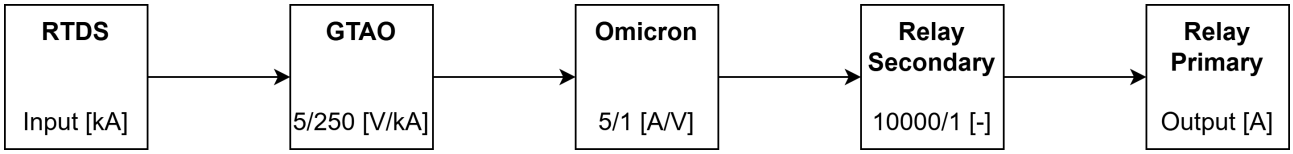

(b) LV-Side

Figure 17: Amplifier chain from simulation to the protection hardware.

Many parameters of the Siprotec 4 7SD5 are restricted to a safety range which depends on the secondary current of the CT and the conversion rate of the relay. Current measurements with magnitudes that are too low cannot be registered in the relay. Parameters are limited with a minimal value to prevent erroneous behaviour due to measuring errors.

The relay settings intended for use during the testing procedure fall below this limit. Therefore, the conversion rate of the secondary rate should be set as low as possible to overcome this limitation, which is why another conversion rate must be scaled to ensure this does not affect the final desired scaling of 1:1. The ratios of the Omicron amplifier are fixed, so the GTAO setting is adjusted to the lowest limit whilst still adhering to other limiting factors, such as signal clipping.

6.1.3 Relay configuration software DIGSI

DIGSI®4, a piece of software, is designed as the user interface to configure the parameters and read the measurements of Siprotec devices [18]. DIGSI boasts a variety of functionalities; only the relevant features are discussed. The noteworthy functions are:

- The configuration of numerous protection parameters.
- The generation of trip and event logs.
- The representation of the analogue measurements and digital event readouts in Siemens' custom-tailored graphical interface SIGRA.

Protection-specific configuration options can be performed through the "General Device Settings" window. This window contains a list of activated protection schemes that can be customised. Each protection scheme has a panel offering various scheme-specific functionalities. The list of the protection schemes and the configuration window of 'Differential protection' can be seen in Figures 18a and 18b, respectively.

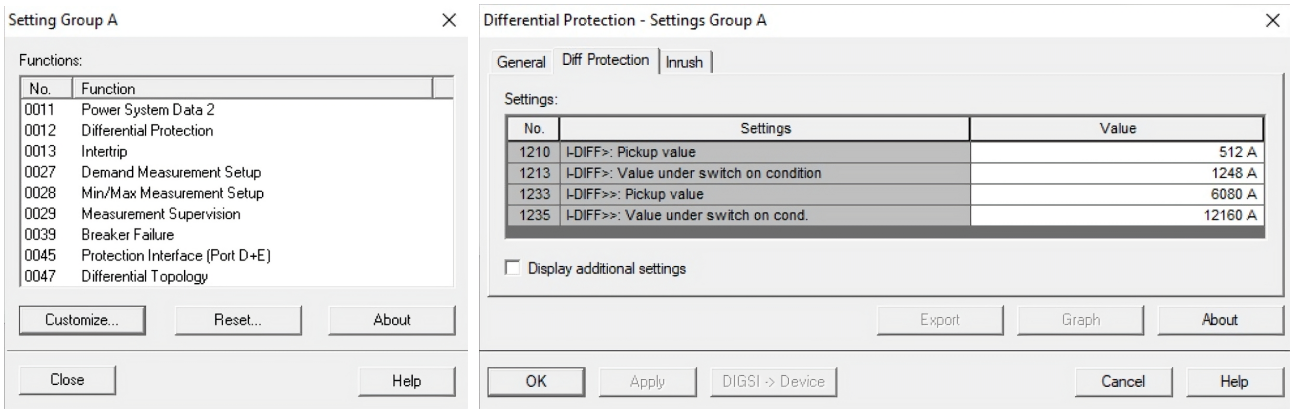

(a) List of configuration windows.

(b) Differential protection parameters configuration window.

Figure 18: Configuration interface of DIGSI. The left pane displays the list of available protection functions, while the right pane shows the configurable parameters for one such scheme.

Furthermore, DIGSI tracks all events registered by the device. In the context of DIGSI, many operations and occurrences are defined as events. As there is an extensive list of events, only a few are given as an example: line closures, fault detection using differential protection, the transmission and reception of trip commands to and from another relay, and the activation of harmonic inrush blocking. All events are time-stamped and chronologically ordered to allow easy investigation and debugging when a fault occurs.

The relay creates a history of events in two ways: the event log and the trip log. The former stores all events in a buffer, which can be accessed through DIGSI. Old data will be expelled from the buffer when it is full, once new events are registered. The latter manner captures only once a fault is active and the relay is triggered. After the fault is cleared, the events are compiled into a unique trip log.

An example of a trip log is given in Figure 19.

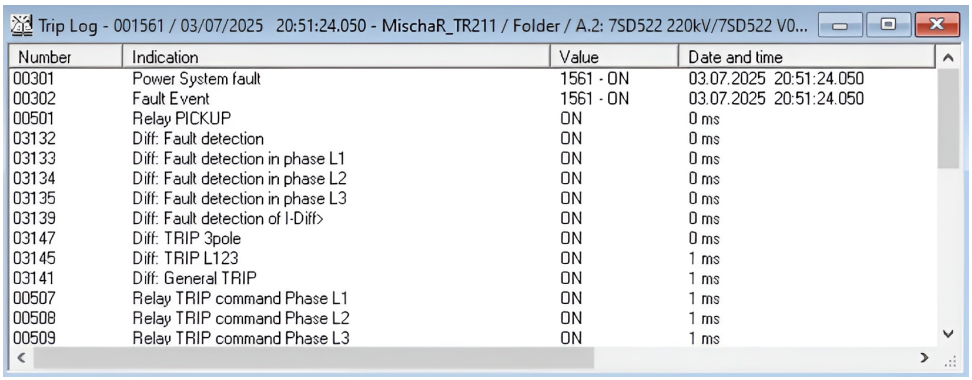

Figure 19: Example of a trip log in DIGSI generated by the relay after a fault.

The final functionality of DIGSI explored in this thesis is the oscillographic representation of analogue measurements. Current waveforms are measured in two ways: by manually commanding the relay to capture, or automatically when a fault is detected. The software used to display the signals is named *SIGRA*.

Besides, the waveform representation with time on the x-axis and magnitude on the y-axis, SIGRA offers a variety of other visualisations. For example, measurements can be visualised as vector diagrams, circle diagrams and as a harmonic component decomposition. Events can also be represented in a binary graph. Finally, multiple signals can be combined in the same file for a comparison.

6.2 Equivalent system model

The graphical user interface used to interact with RTDS is called *RSCAD®FX* [19]. RSCAD is software that runs on a standalone computer, allowing configuration, execution, and analysis of real-time simulations. This section explains how the simulation is composed of a wide range of components, models, and libraries offered by RSCAD.

6.2.1 Grid components

Several library components, which are the building blocks of the model, are used, namely: the source, transformer, cable, CB, CT, and fault components. Finally, various custom functionalities are implemented using logic blocks. These functionalities are organised into hierarchical boxes to improve model clarity. The graphical representation of the described components and the hierarchy boxes is shown in Figure 20.

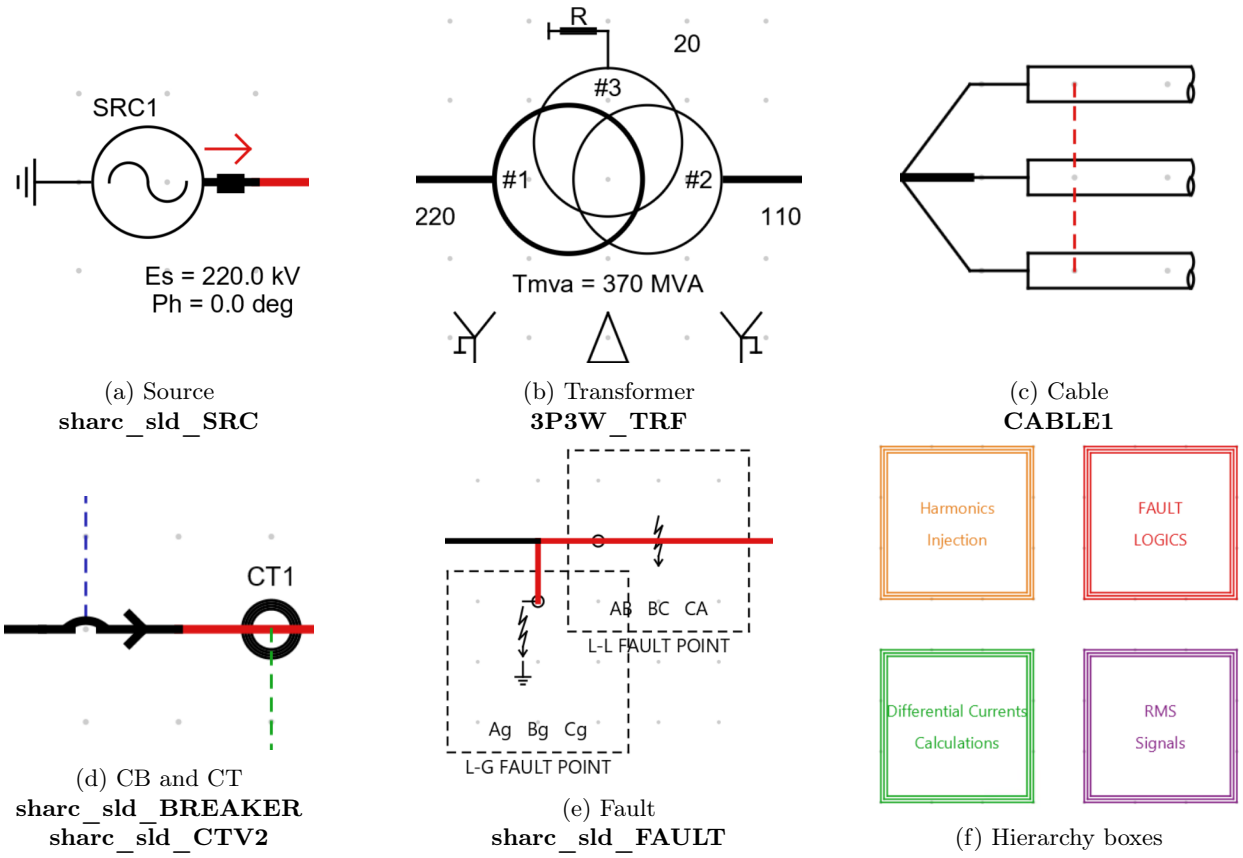

(a) Source
sharc_sld_SRC

(b) Transformer
3P3W_TRF

(c) Cable
CABLE1

(d) CB and CT
sharc_sld_BREAKER
sharc_sld_CTV2

(e) Fault
sharc_sld_FAULT

(f) Hierarchy boxes

Figure 20: RSCAD simulation components utilised in the equivalent system model with their component.

Information about the characteristics of the real-life components is required to model the system accurately. The real-life information of some components is extracted from a variety of documents:

- **Cable:** Positive-sequence impedances and zero-zequence impedances *from test report* [4].
- **Transformer:** BH-curve, leakage reactances, copper losses, and no load losses *from test report* [5].
- **CT:** Resistances and turns ratio *from manufacturing and test reports* [6, 7].

A few components are missing from the list. Firstly, the CB is not included because detailed characteristics of the CB, such as arc currents and open and closed breaker resistances, fall outside the scope of this project. This is because there was no nonlinear arcing visible in the current waveforms. Next, the source and fault characteristics are also not present in the list because they are not static. These characteristics are not derived from a report, but rather result from the system conditions present at the time of the fault. The details of the two components, such as voltage time constants, source zero-sequence impedance, and fault resistances, are derived through determining sequence component models, calculating fault currents, and comparing them to the currents at the actual fault.

Calculation of impedances through sequence component models

In 1918, Charles Legeyt Fortescue presented a paper [20, 21]. In the paper, it was shown that any set of N unbalanced phasors can be represented as the sum of N symmetrical sets of balanced phasors, given that N is a prime number. Using this mathematical breakdown method, three unbalanced phases of a power system can be split into three independent sources, allowing the analysis of asymmetrical faults in power systems.

A sequence-component decomposition is performed on the network segment, and the equivalent circuit of the sequence components can be found in Figure 21.

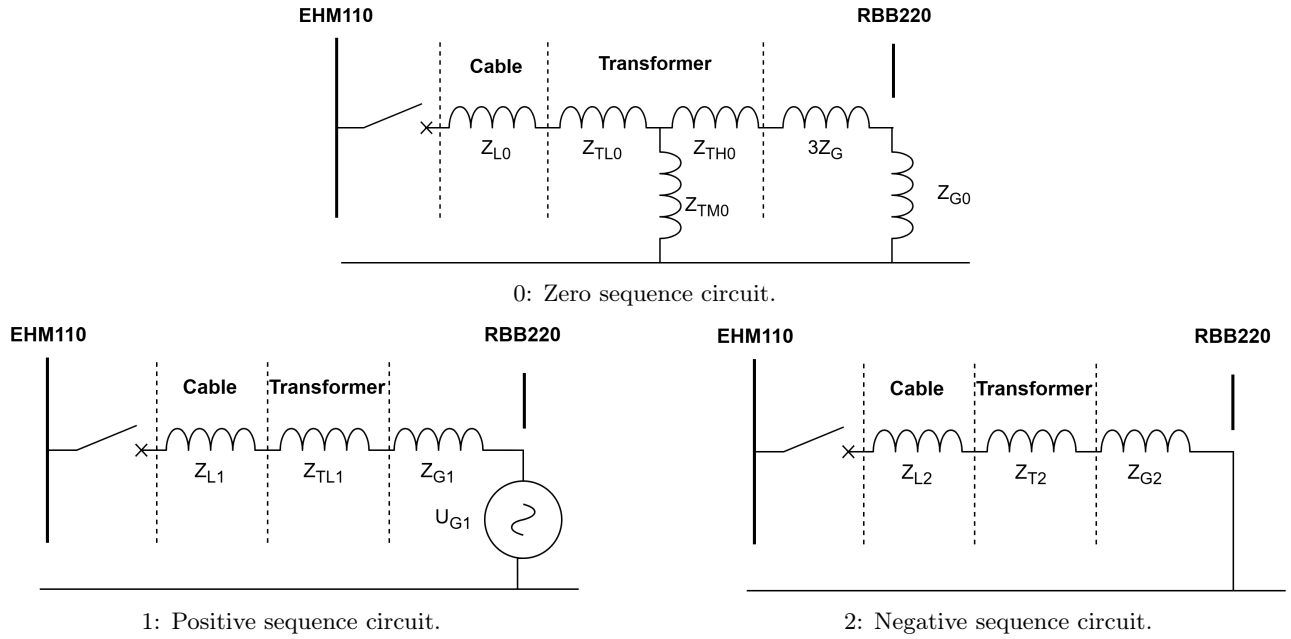

0: Zero sequence circuit.

1: Positive sequence circuit.

2: Negative sequence circuit.

Figure 21: Sequence components representation of the network segment with closed LV side breaker.

The fault current and voltage magnitudes and phases depend on the type of fault. The different signals can be calculated by combining the sequence components in different variations. For example, a fault-ground terminal pair might be left as an open circuit, or it could be connected to another fault-ground terminal pair representing a parallel connection. An overview of the different fault scenarios is provided in Figure 22.

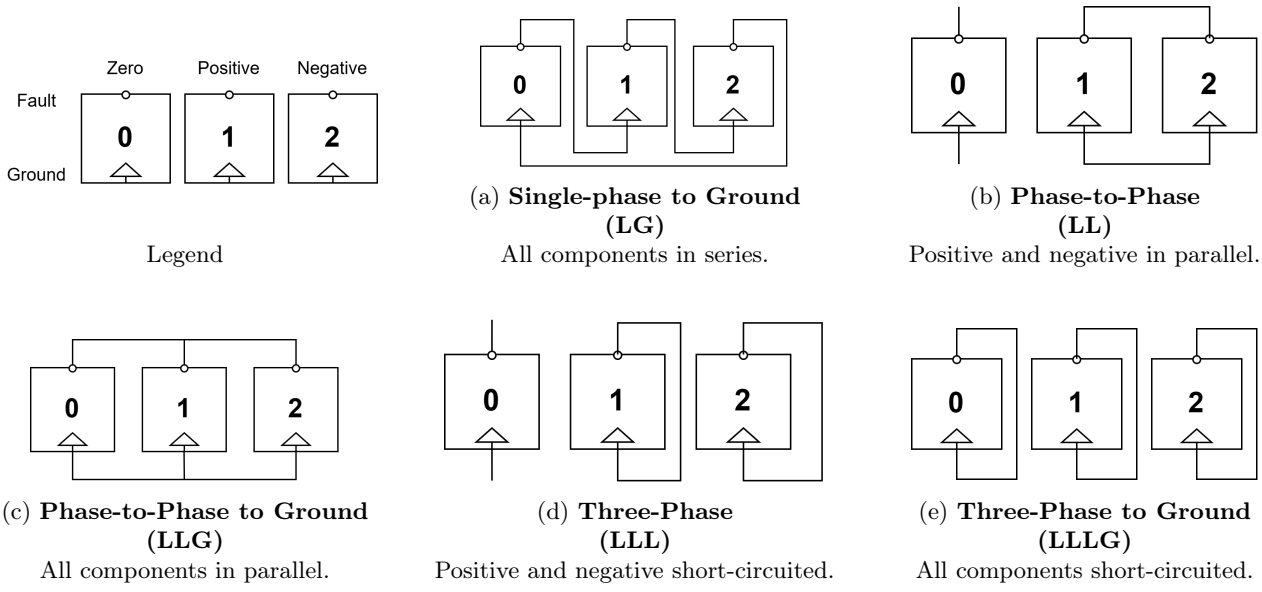

Legend

(a) **Single-phase to Ground (LG)**
All components in series.

(b) **Phase-to-Phase (LL)**
Positive and negative in parallel.

(c) **Phase-to-Phase to Ground (LLG)**
All components in parallel.

(d) **Three-Phase (LLL)**
Positive and negative short-circuited.

(e) **Three-Phase to Ground (LLLG)**
All components short-circuited.

Figure 22: Configurations of sequence components under different fault scenarios.

Combining the equivalent sequence component circuit of Figure 21 and the LG fault scenario of Figure 22a, it is possible to recreate the actual fault. The simplified circuit is shown in Figure 23.

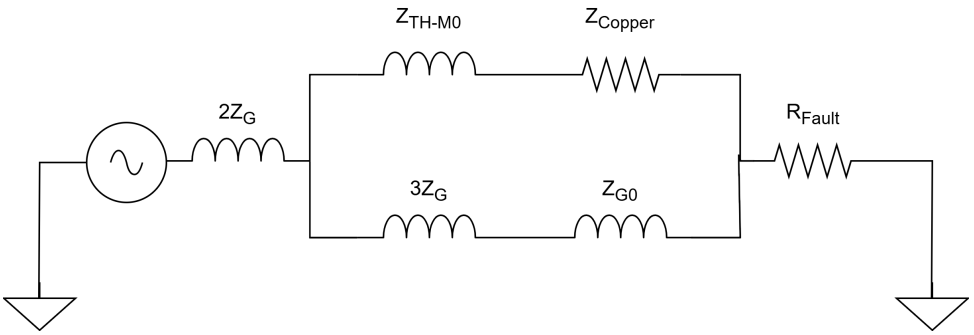

Figure 23: Equivalent sequence component model of a grounded single-line fault.

In Figure 23, two current fault paths can be seen after restructuring the equivalent circuit; the model is simplified to a current divider. The upper path, $Z_{TH} + R_{Copper}$, represents the zero sequence fault current flowing through the transformer windings. The lower path, $3Z_G + Z_{G0}$ is the zero sequence ground current (3I0).

These impedances can be fine-tuned to reach the desired current flowing within the circuits. Firstly, the generator impedance Z_G can be implemented as a combination of resistive and inductive components. The options are: a resistance R, an inductance L, resistance and inductance in series $R + L$, and resistance and inductance in parallel $R||L$. A purely inductive impedance L is chosen for simplicity purposes.

RTDS' software allows for the same type of selection for the zero sequence generator ground impedance Z_{G0}. The selection includes: a short circuit, a resistance R, an inductance L and a resistance in series with a parallel resistance and inductance $R + (R||L)$. A short circuit (i.e. no zero sequence component) is selected to simplify the current ratio between paths.

The fault current magnitude can be calculated by further simplifying the equivalent circuit of Figure 23. In the expression for the fault current magnitude, Z_G is replaced with a purely inductive impedance L, and Z_{G0} is replaced with a short circuit. Then, the formula for fault current magnitude can be expressed as a ratio between R_{fault} and Z_G. This is shown in Equation 7.

$$i_{fault} = \frac{V_{source}}{2Z_G + ((Z_{TH,M0} + Z_{copper})||3Z_G) + R_{fault}} \tag{7}$$

Finally, a relation between the two desired characteristics (i.e. Z_G and R_{fault}) is found by filling in the measured fault current magnitude into i_{fault}. The other necessary variables can be extracted from the transformer test report. The final characteristics are obtained through iterative tuning of simulation parameters to achieve an accurate fault replication.

6.2.2 Artificial harmonic injection

The second harmonic content plays an essential role in the malfunction of the relay. Here, the second harmonic component was artificially added to the fault current to determine its effect without the need for extensive modelling of saturation within the transformer core.

The component is implemented as a 100 Hz signal with customisable phase [°] and magnitude. This new signal is mixed with the fault currents before being transmitted by the GTAO. This signal should only be present when the circuit breakers are closed. The magnitude is dialled to zero whenever the circuit breakers are open to achieve this. Furthermore, the length of time the harmonic component is active can also be customised to observe the impact of diminishing harmonics over time.

The saturation of the transformer core was also modelled by providing an approximate characteristic. This simulation function almost became redundant when a more accurate 2nd harmonic content generator was added. However, one use case remained for this function, namely to model the effect of external harmonic contributors to the relay, which were present during the original fault.

6.2.3 Circuit breaker closing logic

Proper attention has been given in Chapter 5 to the importance of the CB closing angle. The closing angle determines the magnitude of the DC component within the fault currents. A scheme has been imagined to ensure the proper closing angle of the CB. Moreover, this scheme is similarly used for fault activation.

First, one of the phases is selected as the reference phase, which is phase A in the simulation. All actions will be performed synchronized to this phase. Voltage measurements will be taken before the CB outside the protected region. Whenever a close command is issued, the simulation will wait until the reference phase passes the 0-voltage crossing in the positive direction.

The CB closes after the desired time Δt has elapsed. To make the simulation more comprehensible, Δt is converted from degrees phase [°] through the unit conversion: $\Delta t[s] = \frac{\text{phase } [°]}{360[°] \cdot f[Hz]}$. The phase is expressed in degrees and it is an input to the simulation to specify the desired closing timing.

The flowchart representing this scheme is shown in Figure 24a, accompanied by a graphical representation in Figure 24b.

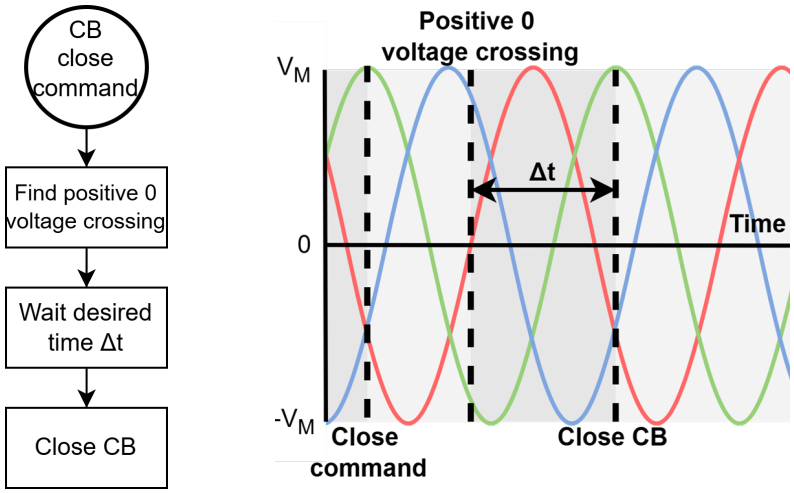

(a) Flow chart (b) Graphical representation

Figure 24: Scheme to precisely ensure the simulated CBs are closed at the desired time.

6.2.4 Quantifying the response type through a fault timer

To identify the type of response, the system model includes a timer that functions as a fault stopwatch. The timer is started at the fault inception time and stopped once a trip command is received from the relay. A flow chart of a scheme can be seen in Figure 25.

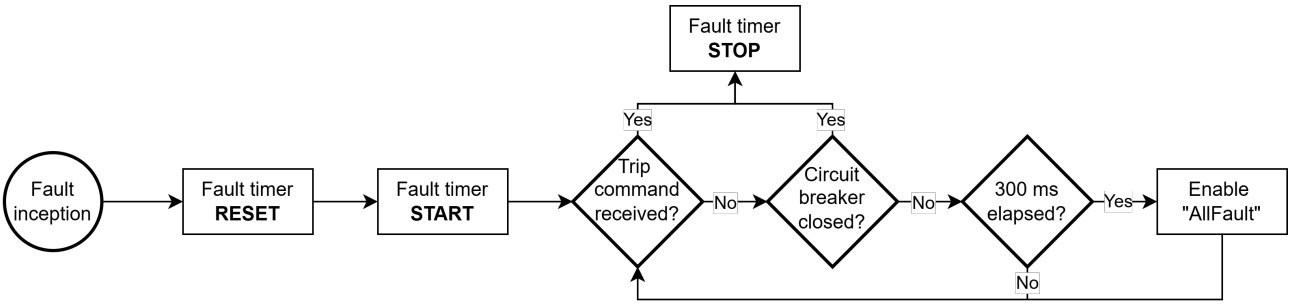

Figure 25: Flowchart of the *fault timer* used to get the response time of the relay.

Due to the subject of this paper, there will be instances when the relay fails to send a trip command upon introducing a fault; this constitutes a malfunction. However, it is preferable to capture the signals with the relays to investigate the response. Moreover, this needs to be done inside the capture window of the relay. The

relay is limited to capturing the current waveform 500 ms before the moment the relay is triggered. To ensure that the relay is triggered promptly, the simulation produces a fault in all phases, 300 ms after the initial fault inception. The activation of all phases is named *AllFault*.

Manually stopping the timer should be an option for rare cases when the relay never triggers, even after the AllFault. In these cases, CBs can be closed manually using an input. The model should then recognise the closing of the CBs and stop the timer.

Figure 26 shows the current waveforms when the relay maloperates. Here, the AllFault operation can be observed at the end of the waveforms, as indicated by all phases reaching an extreme current magnitude. The vertical black line at t = 0.00 is the moment the relay reacts.

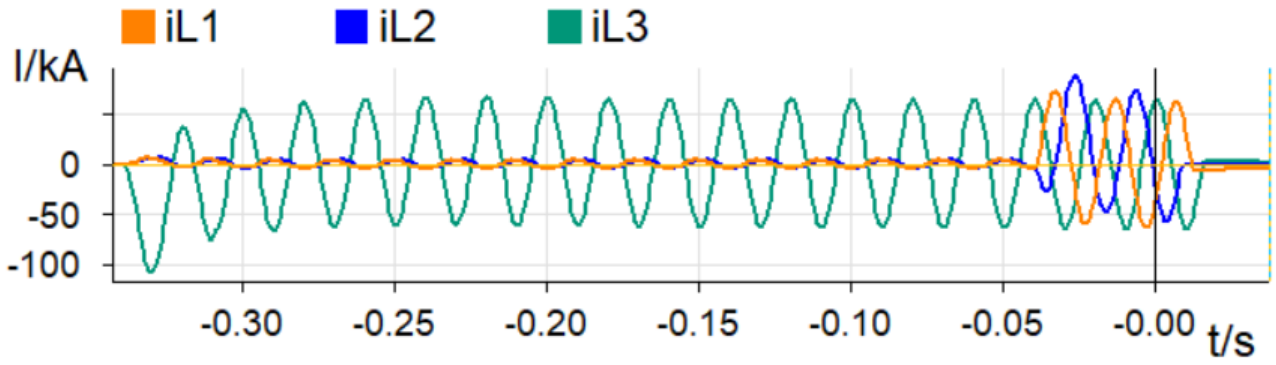

Figure 26: DIGSI export of the fault replication. After 300 ms, all phases are faulted to ensure the desired waveform is captured.

In this manner, the relay reaction can be quantified using the fault timer. Fast times indicate a correct response, while slow response times indicate a malfunction.

6.2.5 RSCAD Dashboard and configuration windows

A custom dashboard with multiple configuration windows is designed to provide a clear overview of the simulation's current state and to configure simulation-specific parameters easily. This dashboard can be viewed in Figure 27.

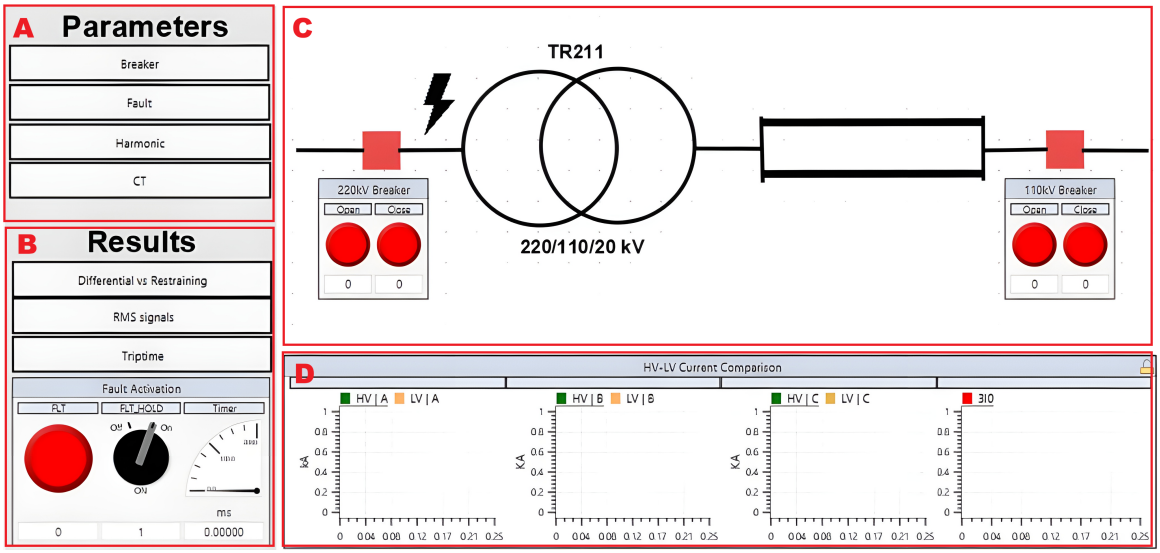

Figure 27: Custom RSCAD dashboard designed to configure, control and monitor the simulation.

The dashboard is divided into four panels. Panel A contains the parameter configuration windows for several simulation features, including CBs, fault inception, artificial harmonics, and CTs. Panel B contains the results of running the simulation. The results are presented using a variety of graphs and the fault timer. Panel C is

the single-line diagram of the network segment, showing the real-time statuses of CBs, along with buttons to open and close them. Finally, panel D contains graphs that compare the current on the HV and LV sides per phase, as well as a graph of the ground current 3I0.

6.3 Verification of the system model

Figure 28 shows a comparison of all phases of the original and the replicated malfunction current waveforms.

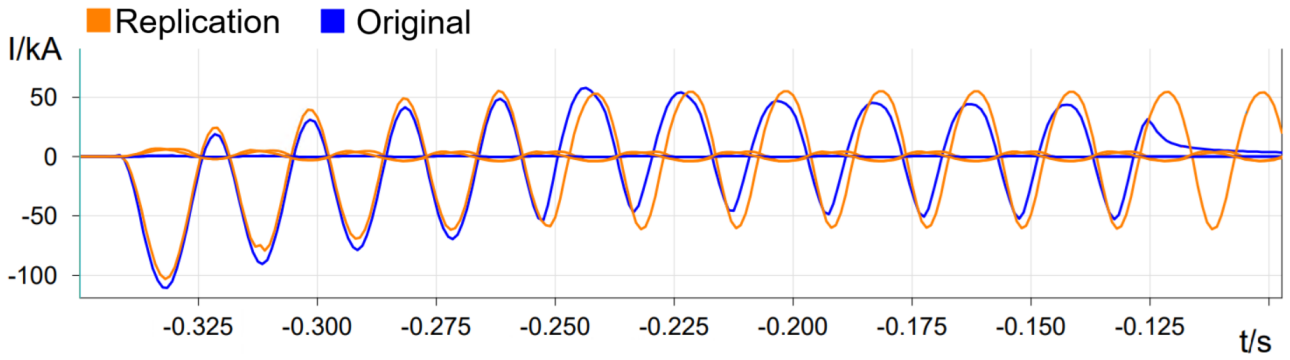

Figure 28: A comparison of the original and the replicated fault current waveform of all phases.

There are several differences between the replicated and the original signal. Most notable differences include: 1) At roughly t = -0.250 s (i.e. 80 ms after fault inception), the magnitude of the original drops and experiences a phase shift. 2) The original fault is isolated approximately at t = -0.125 s, the replicated signal has a later pickup time due to the AllFault function.

One visible difference is the current dip and phase deviations 80 ms after the CB was closed. During the original fault, the protection mechanisms of a surrounding network segment tripped at this moment. This has not been implemented in the equivalent system model because its effect on the malfunction is irrelevant. This is because the malfunction exists in the test setup without the implementation of the current dip.

The CBs of the original fault were closed approximately at t = -0.125 s; the fault in the replicated signal persists. In the trip logs from the fault event, it can be seen that the distance protection tripped the relay during the original fault. Therefore, the relay not tripping is an acceptable deviation because the implemented distance protection is not considered in this case study.

In conclusion, the equivalent system model proves to be a sufficient replication of the original fault, regardless of the visible deviations. The HIL model is capable of recreating fault situations in which the Siemens Siprotec 4 7SD5 is susceptible to malfunctioning. Moreover, different fault circumstances can be simulated to test the robustness of any proposed solutions.

7 Test Procedure and Methodology

In this chapter, the previously built system model is applied to determine the relay configuration that is more resilient to the presented malfunction of differential protection. The data obtained from the protection operation, which is integrated in the HIL simulation, will help to propose recommendations for improving the longevity and security of the affected network segment and others like it.

First, Section 7.1 defines a priority list of tests to be conducted. In this order, obsolete or redundant tests can be avoided due to time constraints. Section 7.2 will explore the five test cases that are constructed to test the Siprotec 7SD5. Finally, Section 7.3 explores the test procedures under various fault circumstances, including location, scenario, and condition. These steps are necessary to test the robustness of any proposed recommendation.

As a preamble, two terms used throughout this chapter are defined for clarity. First, "*condition*" refers to the state of the network segment when the fault occurs. Second, the term "*circumstances*" denotes the collection of fault characteristics, such as fault locations, scenarios, and conditions.

7.1 Testing priority List

Since not all tests are equally relevant, test cases will be performed according to a priority list. This list begins with circumstances that resemble the original fault, which is the closest, and gradually builds up to determine whether the malfunction occurs during other potential fault events. Using this process, lower-priority tests can be preemptively excluded if they are deemed unlikely to yield meaningful results. The priority list is as follows:

1. Testing the response of the closest replication to the actual fault using the Siprotec 4 7SD5 (i.e. a LG-fault that occurred at the HV side of the transformer before energisation).
2. Testing the response with the relay parameters that were designed to be used for this network topology; however, they have never been implemented for unknown reasons.
3. Testing three relay configurations for the actual fault, where only one parameter is altered per variation.
4. Repeating the first three items on this list with other fault circumstances, such as:
   (a) **Locations**: Where the fault occurred.
   (b) **Scenarios**: What type of fault occurred.
   (c) **Conditions**: In what state the network segment was when the fault occurred.

7.2 Test cases with the relay Siprotec 4 7SD5

This section explores five different test cases. Case A is the recorded configuration from the relays in the affected field. Case B is a configuration of the relays that was not implemented. The configurations of Cases C through E are variations of Case A. For each of these cases, a single parameter is carefully selected from the downloaded configuration and varied to find a configuration where the malfunction does not occur. The chosen parameters are: 2nd harmonic in % of fundamental (Setting 2302), the time for Crossblock with 2nd harmonic (Setting 2310), and the I-DIFF» value under switch on condition (Setting 1235).

The test cases comprise simulations with the replicated faulty waveforms with different relay parameter configurations. Each case is simulated 20 times to account for the random results of the protection operation. Additionally, the relay's reaction to both faulty and non-faulty conditions is equally essential; correcting the malfunction must not impair the relay's ability to operate normally.

A detailed summary of the test cases can be found in Table 4.

Table 4: Summary of the test cases.

Case	Name	Description
A	Downloaded configuration	The relay parameters that were configured on the relays when the original fault occurred.
B	Setting statement configuration	The relay parameters that were designed to be utilized in the field written in a TenneT document [8].
C	2nd harmonic threshold	A variation on Case A, where the "2nd harmonic in % of fundamental" parameter (Setting 2302) is varied. It is set to 10%, 25%, 35% and 45%.
D	Crossblock period	A variation on Case A, where the "Time for Crossblock with 2nd harmonic" parameter (Setting 2310) is varied. It is set to 0, 0.03, 0.06, and 10 seconds.
E	I-DIFF>>switch threshold	A variation on Case A, where the "I-DIFF>>under switch on condition" parameter (Setting 1235) is varied. It is set to 6080, 8160, and 10240 A.

Further elaboration on the procedures and reasoning behind the test cases mentioned in the table will be provided in their respective sections.

7.2.1 Cases A and B: downloaded and setting statement configurations

The first two test cases will investigate the relay's reaction when configured with two specific configurations designed for this network segment. Test case A is downloaded from the relay, and test case B is extracted from a TenneT official document.

Test case A shows the settings extracted from real-life relays. Following the incident, a comprehensive investigation was conducted to determine the cause and consequences of the fault, as well as to provide recommendations on how to prevent similar faults from occurring in the future. To support these investigations, all relevant data were downloaded from the relays, including a log of all events that occurred before and during the fault, a log of all triggered digital events, analogue fault current measurements, and the relay configurations.

Test case B shows all the parameters of the document named the *setting statement* [8], designed explicitly for this network segment. The setting statement is an official document developed in 2019 by protection engineers at TenneT, wherein all the parameters for the relay configurations are calculated, explained, and summarised.

As the relay has over a hundred configurable parameters, all of which are fully explained in the relay's manual, it would not be possible to describe each parameter separately. However, all relevant parameters surrounding the differential protection principle and their configured values for Test cases A and B are highlighted in Table 5 to illustrate the key differences between the two configurations.

Table 5: Relevant Siprotec 4 7SD5 differential protection parameters for test cases A and B.

No.	Settings	A: Downloaded	B: Setting Statement
1210	I-DIFF >: Pickup value	300 A	320 A
1213	I-DIFF >: Value under switch on condition	1250 A	320 A
1233	I-DIFF >>: Pickup value	6000 A	2880 A
1235	I-DIFF >>: Value under switch on condition	12250 A	2880 A
2301	Inrush Restraint	ON	OFF
2302	2nd harmonic in % of fundamental	15 %	15%
2305	Maximum inrush-peak value	8500 A	4160 A
2310	Time for Crossblock with 2nd harmonic	∞ s	0.06 s

There are several differences between the two configurations. Firstly, the setting statement does not use the "Value under switch on condition"- Settings 1213 and 1235 are identical to 1210 and 1233, respectively. Secondly, the pickup values for the I-DIFF>> function (Setting 1233 and 1235) are significantly higher in the downloaded configuration. Third, "Time for Crossblock with 2nd harmonic" (Setting 2310) is set to its

maximum value in the downloaded configuration, whereas a more reasonable value is selected in the setting statement. Finally, the "Inrush Restraint" (Setting 2301) is disabled in the setting statement.

7.2.2 Cases C, D, and E: variations on the downloaded configuration

Examination of the trip logs and event logs from the original fault and comparison of the downloaded data with the configuration from the setting statement revealed that several key events can identify the relay fault. The key events are *harmonic inrush detection*, *all phases blocked simultaneously (i.e. crossblock)*, and the *I-Diff>> function triggering*.

Three test cases simulate variations of the downloaded configuration from Test case A to identify which of the key events described lead to the malfunction. Each key event has an associated setting that are tested; these are Settings 2302, 2310 and 1235. The expected results for each test case are described below.

Case C: 2nd harmonic threshold

By investigating the trip log of normal operations and malfunctions, it was demonstrated that the 2nd harmonic content detection functionality restrains relay operations during every malfunction. A logical conclusion would be that the harmonic threshold is set too low, and raising it would eradicate the malfunction.

This assumption will be verified by altering the downloaded configuration by varying Setting 2302, the 2nd harmonic detection threshold. The following values will be examined: 10%, 20%, 25%, and 30%. The hypothesis is that high threshold values will prevent malfunction, and low threshold values will increase the likelihood of a malfunction.

The 2nd harmonic percentage of the original fault throughout its entire duration is roughly 15% - 20% in one of the non-faulted phases. Therefore, the relay is expected to trip correctly at high settings. This test case aims to verify whether this expectation is true.

Case D: crossblock period

The crossblock functionality appears to be a promising parameter to adjust to prevent the malfunction. The non-faulty phases experience relatively significant amounts of harmonic content, whilst the faulted phase is not distorted above the threshold.

The downloaded configuration has Setting 2310, the time for crossblock with 2nd harmonic, set to infinity. This excessive time could always restrain operations if the harmonic threshold is exceeded. A lower value should be chosen to counteract this. Alternative values for this setting tested inside this case are: 10 s, 0.06 s, 0.03 s, and 0 s. The last case would be the same as disengaging the crossblock functionality.

The original fault lasted 189 ms. Throughout this fault, all phases were (cross)blocked due to the harmonic inrush restraint. By setting the crossblock period to a lower value, it is expected that the relay will trigger after the parameter time has elapsed. For example, if Setting 2310 is set to 0.03 s, the relay is expected to react after 30 ms.

Case E: I-DIFF>> switch threshold

Comparing the downloaded and the setting statement configuration reveals a considerable difference in Setting 1235, "I-DIFF>>: Value under switch on condition"; this parameter is more than four times larger in the default configuration. Moreover, the event log of the fault revealed that the tripping of the relay was a reaction of the I-DIFF>> function, and not the I-DIFF> function.

The setting is varied between a couple of values to determine the influence of this parameter. Siemens recommends configuring Setting 1235 to a value between five and six times the rated current of the circuitry [3]. The selected setting value is gradually reduced from the original value of Test case A to the recommended value. The values to be selected are: 10240 A, 8160 A, 6080 A, and 2880 A. The value of 6080 A is the same as the non-switched-on condition (Setting 1233) of the downloaded configuration, and 2880 A is the same as Setting 1235 in the setting statement.

The expected result of this test case is the correct operation of the relay for lower values of this parameter. The lower setting increases the selectivity of the I-DIFF>> function so that it will increase the chances of it

operating during the fault. However, too low values of the setting might cause nuisance tripping during normal energisation.

7.3 Applying test cases to different circumstances

Since different faults might also produce slow and erroneous reactions, the network segment must be thoroughly simulated and tested to identify potential undiscovered vulnerabilities. The simulations are set to different fault circumstances to attempt to reconstruct the malfunction. Three fault circumstances will be considered, namely: *location*, where the fault occurred, *scenario*, what type of fault occurred, and *condition*, what state the network was in when the fault occurred.

7.3.1 Locations

Figure 29 gives an overview of possible fault locations concerning the protected area.

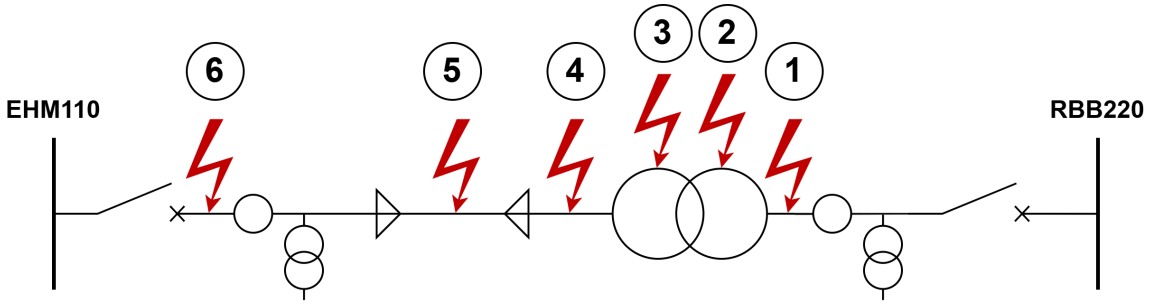

Figure 29: Possible fault locations in and outside the protected region.

The following list provides a breakdown of the various fault locations considered in the analysis:

- **Location 1** corresponds to the point where the actual fault occurred, namely, outside the HV side of the transformer, electrically the closest to RBB220 whilst remaining in the protected region.
- **Location 2** represents an internal fault within the HV winding of the transformer.
- **Location 3** represents an internal fault within the LV winding of the transformer.
- **Location 4** refers to a fault occurring beyond the high-impedance transformer at the LV voltage level.
- **Location 5** denotes a fault located anywhere along one of the cable bundles.
- **Location 6** indicates a fault situated outside the protected region in or close to EHM110. The protection system should not respond to faults at this location; instead, it serves as a reference to verify correct relay behaviour under external fault conditions.

The largest current amplitude is expected for location 1, as this is the closest possible fault location to the CB that is closed during energisation. The farther away a fault is, the lower the expected current magnitude is. A transformer has a relatively high impedance when compared to other grid components. Therefore, the high impedance reduces the current drawn when the fault occurs behind the transformer.

The equivalent system model does not support internal winding faults, such as locations 2 and 3. With RTDS, it is possible to recreate such faults with custom components [22, 23]. However, this falls outside the scope of the project due to a lack of the necessary data to model the internal structure of the transformer. Unfortunately, this means that locations 2 and 3 will not be considered in this report.

7.3.2 Scenarios

Different fault scenarios should be examined as they have a significant impact on the amplitudes of the fault currents. In addition to the LG fault, the simulation must be capable of Phase-to-Phase (LL), Phase-to-Phase to Ground (LLG), Three-Phase (LLL), and Three-Phase to Ground (LLLG) faults. Different current waveforms and reactions are expected because each scenario has a unique configuration of sequence components. The expected waveforms of all scenarios can be seen in Figure 30.

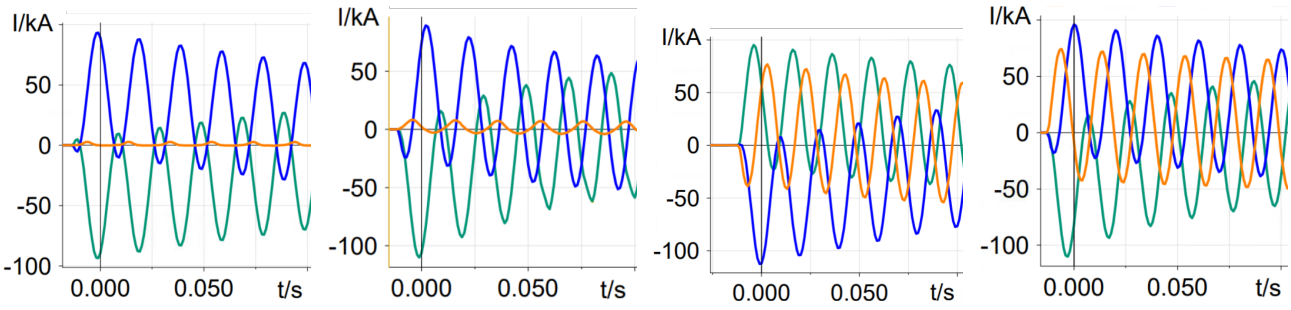

(a) LL (b) LLG (c) LLL (d) LLLG

Figure 30: Expected current waveforms for all scenarios.

7.3.3 Conditions

Finally, it is necessary to consider different starting conditions, as various time-varying processes are involved, such as the energisation of a transformer. Therefore, three conditions are proposed: 1) The fault exists before energising the HV-side. 2) The fault occurs after the energisation, but before the LV-side breaker is closed, and 3) The fault is activated in steady-state conditions; both breakers are closed and enough time has passed since the energisation.

There are two differences depending on the condition of the grid segment. Firstly, the relays will use the default threshold values, Settings 1210 and 1233, instead of the "under switch on condition" values, Settings 1213 and 1235, when the grid segment has been energised. Secondly, the current magnitude will change when the LV side CB has been closed. Instead of the fault being fed from only one side, it will be supplied from both sides.

Conditions 2 and 3 can be excluded in specific test cases. For example, if the proposed relay configuration causes tripping during a non-faulty energisation, it becomes unnecessary to test for malfunction under steady-state conditions.

Any combination of the aforementioned factors could result in a correct fast or faulty slow response. In total, over 25.200 tests need to be executed when considering all possible arrangements. However, a full combinatorial coverage will not be required. By working down the priority list, some tests can be ruled out if they are deemed obsolete. Table 6 summarises all testing-related circumstances, including all locations, scenarios, and conditions.

Table 6: Summary of different factors influencing the simulation.

Location	**Scenario**	**Condition**
1: HV side transformer	a: LG	Pre-energization
2: HV internal winding	b: LL	HV-side breaker closed
3: LV internal winding	c: LLG	Steady-state
4: LV side transformer	d: LLL	
5: Cable	e: LLLG	
6: Outside protected region		

In conclusion, several test cases are proposed to find a more optimal relay configuration. Each test case focuses on a specific relay setting to see its effect on the malfunction. Furthermore, a priority list is defined to eliminate unnecessary tests efficiently. Finally, all combinations of fault circumstances are applied to the test cases to test the robustness of any proposed solution.

8 Analysis of Results and Discussion

The test procedures alone are insufficient to determine an optimal relay configuration. Therefore, a thorough analysis of the results is necessary to recommend improved settings. This chapter analyses the results of the individual test cases and assesses how different fault circumstances influenced the outcomes. Finally, a recommendation is provided on which settings should be configured and which should be avoided.

In Section 8.1, three types of relay responses are defined and employed as metrics to assess whether a result is a malfunction. Then, the defined metrics are used in Section 8.2 to investigate the test cases under the original fault circumstances. Further, Section 8.3 builds on this foundation by exploring the defined circumstances and identifying those most susceptible to faults. Finally, a suggestion is proposed in Section 8.4 to prevent future malfunctions. Potential unintended consequences of adjusting relay settings are also discussed.

8.1 Determining the type of relay response

After performing the testing procedures, three types of trip reactions to initiating a fault event were observed. The three types of responses are: trip (<45 ms), delayed trip (45-300 ms) and no trip (>300 ms). The Siprotec 4 7SD5 is rated to respond between 35-45 ms [3] for a fault detected with differential protection. The upper boundary of this range is considered the upper limit for normal relay tripping. The no-trip boundary begins at 300 ms, as this is where the AllFault functionality begins.

The relay first detects the closure of the CBs. The *line closure* event can be detected through a variety of methods, namely through current and voltage measurements or manually through binary signals. The relay's behaviour changes depending on the detection of a line closure, typically making it less sensitive to tripping. Settings 1213 and 1235 serve as examples of this behaviour.

The type of response that occurs depends on whether two events occur within the relay: *I-DIFF>>response* and *2nd harmonic detection*. The first response - defining event is checking if the I-DIFF>>functionality responds. It is expected to always operate due to the excessive magnitude of the differential current. The reaction is labelled as a malfunction if the I-DIFF>>functionality does not operate.

Naturally, a malfunction is undesired. Nevertheless, the severity and length of the malfunction depend on the amplitude of the 2nd harmonic within the measured fault currents. The relay will trip when the amplitude does not exceed the configured restraint threshold, causing a *delayed trip* response. However, the relay will not trip if the threshold is exceeded and will only trip once the harmonic level drops below the pre-set threshold.

Figure 31 illustrates a flowchart outlining the sequence of events that can lead to either a correct or incorrect operation.

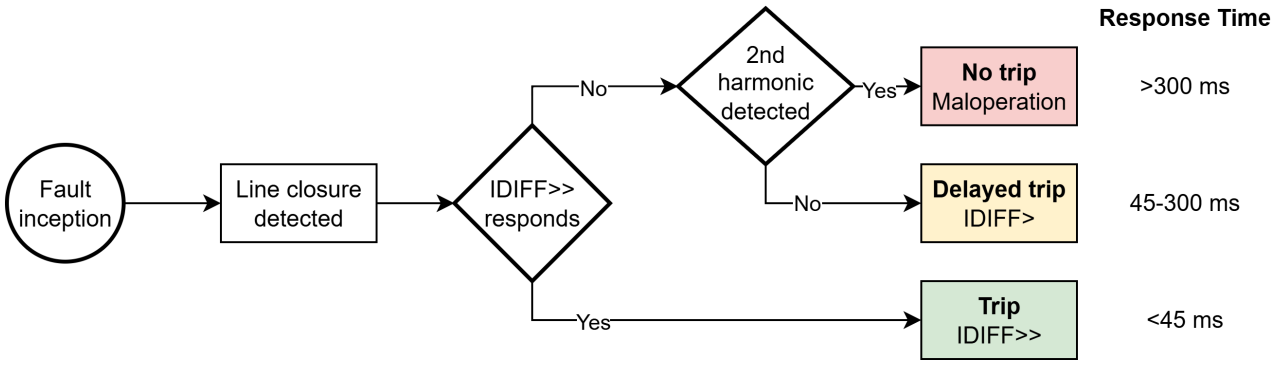

Figure 31: Flowchart showcasing the sequence of events that lead to correct or incorrect relay reactions.

The classification of reaction types can also be understood by visualising it as a timeline. The timeline begins at the instant of the fault inception. The instant when the relay triggers is recorded and classified into one of the three response types. The timeline representation is illustrated in Figure 32.

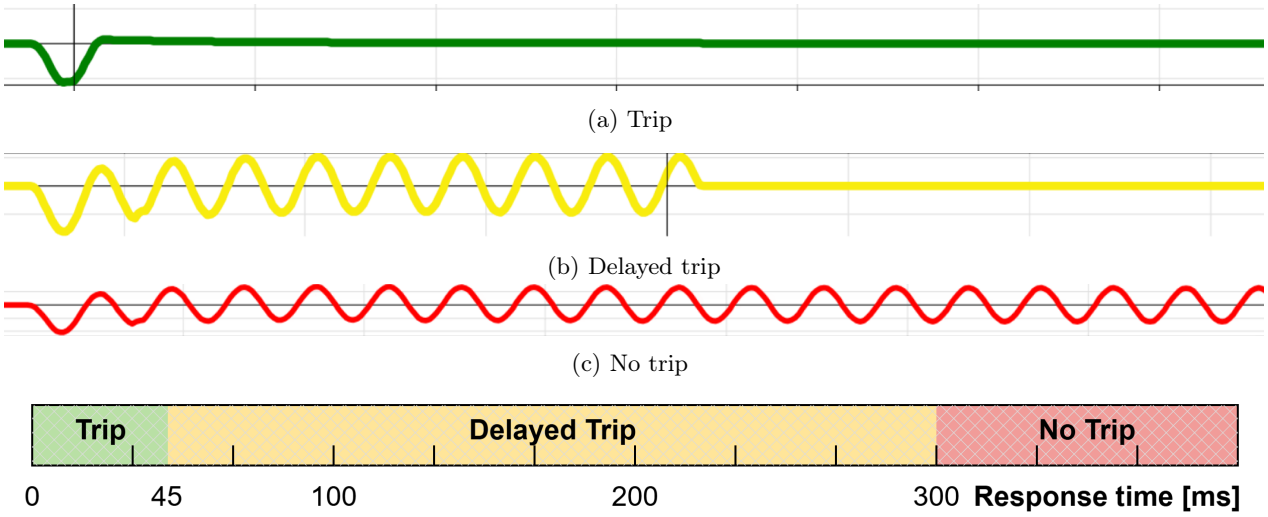

Figure 32: Classification of the relay reaction depending on the relay's response time to a fault.

8.1.1 Confidently dealing with stochastic results

The relay operation is determined to be stochastic. In a malfunction-prone testing setup, the I-DIFF>> function operates stochastically. However, the probability of correct functioning is likely not fixed and could vary depending on different circumstances; in some cases, it might be higher, while in others it may be zero.

It is necessary to run the simulation multiple times for each test case to distinguish the type of relay response, as the malfunction does not consistently occur in every test. By inducing the fault one hundred times and observing the resulting response types, it was concluded that the probability of malfunction is approximately 25%. So, using this approximation, how many unique simulations are required to be able to confidently conclude (at least 95%) that the malfunction occurs with the given relay configurations?

The probability that n tests do not include a malfunction is $P(0 \text{ malfunctions}) = (1-0.25)^n = 0.75^n$. Thus, the condition of the desired confidence being at least 95% can be formulated as $0.75^n < 1-0.95 = 0.05$. Solving the inequality for n gives us Equation 8:

$$n > \frac{log(0.05)}{log(0.75)} \approx 10.41 \tag{8}$$

Therefore, at least 11 tests are required to determine the type of response confidently. However, the assumption that the probability of malfunction under fault-prone circumstances is 25% could be inaccurate, so that the probability might be lower, especially when considering other circumstances. Thus, the number of tests is nearly doubled to 20 to account for this assumption.

8.2 Results of the test cases

It is essential to test and verify the proposed relay configuration for both faulty and non-faulty conditions. The desired outcome of the tests is that the malfunction does not occur during a fault, and that the relay does not trip during normal energisation. This section discusses both conditions for all test cases before identifying the desired results for further testing.

8.2.1 Fault replication for each case

Each test case is tested 20 times using the original circumstances. The reaction to each experiment is discussed. This section aims to find experiments that produce viable alterations to the relay's configuration.

Test case A: downloaded configuration

Firstly, the relay is configured with the downloaded configuration to define the baseline of all tests. The spread of the relay's response time to the replicated fault can be seen in Figure 33.

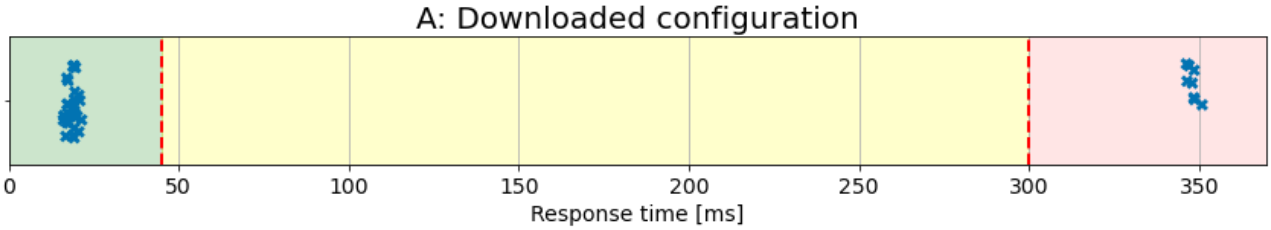

Figure 33: Spread of relay's response time to the replicated fault for Test A.

The baseline experiment performed exactly as expected. For most tests, the relay operated without malfunction. Additionally, the relay generated slow response times in a small portion of the tests, indicating that the malfunction is present when the relay is configured for Test case A.

Test case B: setting statement

Then, the relay is altered to have the configuration of Test case B. The spread of the relay's response time can be seen in Figure 34.

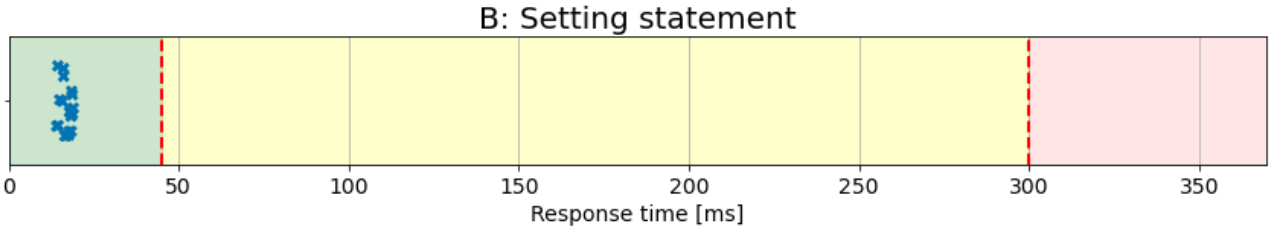

Figure 34: Spread of relay's response time to the replicated fault for Test B.

When the relay was configured with the setting statement configuration, the device managed to trip correctly for all twenty faults during energisation.

Test case C: 2nd harmonic threshold

The relay is configured to Test case C. The performance of the relay's response times under the original fault circumstances is shown in Figure 35.

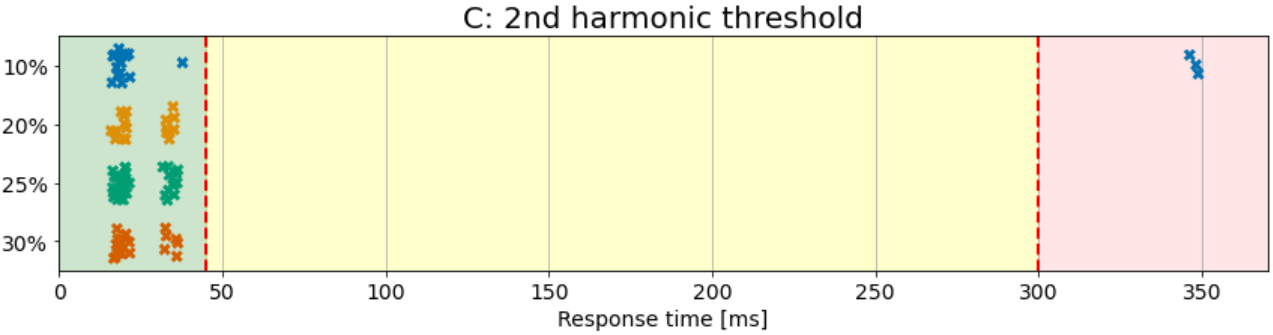

Figure 35: Spread of relay's response time to the replicated fault for Test C.

The results of Test case C show that Setting 2302, the 2nd harmonic threshold has a significant influence on the prompt blocking function of the relay. Higher setting values, such as 20%, 25%, and 30%, contributed to

preventing the "No Trip" response. Investigating the fault log reveals that the I-DIFF> functionality manages to pick up the fault and trigger without being restrained due to the 2nd harmonic inrush restraint. On average, the relay managed to catch the fault below the 45 ms threshold. This response time qualifies as a correct reaction.

Test case D: Crossblock time

The configuration of the relay is set to Test case D. The spread of the relay's response time can be seen in Figure 36.

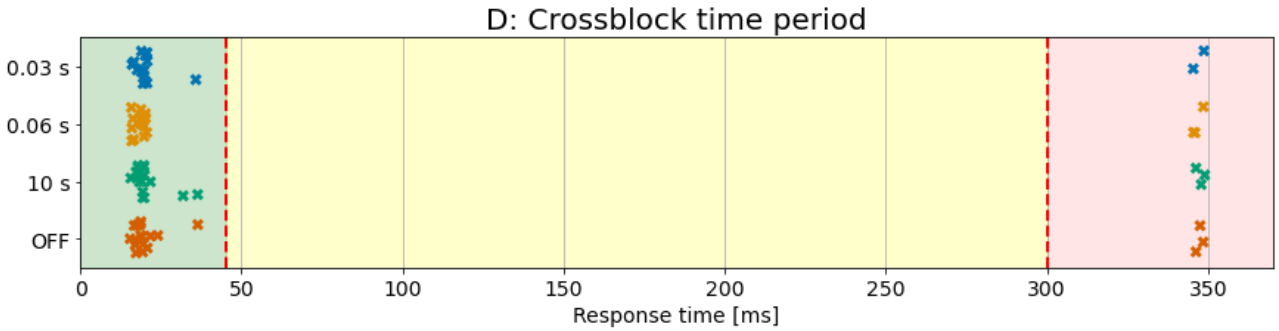

Figure 36: Spread of relay's response time to the replicated fault for Test D.

Test case D generated an unexpected result. Every suggested variation for Setting 2310 did not affect the type of relay reaction. This includes no- and infinite-delay. The unexpected result could have two possible reasons: 1) The crossblock functionality does not operate during the malfunction, and the assumption that it did was incorrect, 2) The crossblock functionality of the Siprotec 4 7SD5 does not work as intended, or 3) The crossblock functionality itself was blocked by another event or function.

The first possibility seems unlikely. It is clear from the trip log that the I-DIFF> function was restrained due to the 2nd harmonic restraint. Moreover, the oscillographic representation reveals that the level of 2nd harmonic content in the faulted phase does not exceed the threshold of Setting 2302. Next, the second possibility is also unlikely as the protection devices are rarely to blame. Finally, the third option could explain the discrepancy. The line closure event significantly alters the relay's reaction and will require a separate investigation.

Nevertheless, the setting does not offer a viable solution to prevent the malfunction and is therefore omitted from further testing.

Test case E: I-DIFF>>switch threshold

Finally, the relay is configured with Test case E. The spread of the relay's response time to the replicated fault can be seen in Figure 33.

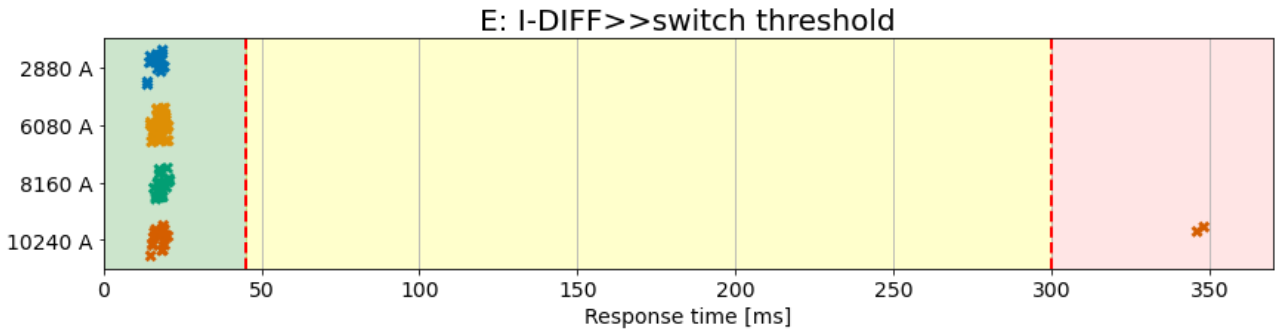

Figure 37: Spread of relay response time for Test E.

The configuration of Test case E successfully prevents the malfunction whilst still allowing the circuit to energise under normal circumstances. It can be concluded that the tests with the I-DIFF>> switch threshold revealed an acceptable solution for the original fault circumstances.

8.2.2 Non-faulty energisations

The response of the relay during normal energisation is yet to be considered. This response is considered, tested, and evaluated in this section.

Non-faulty energisations are evaluated in the simulation by closing the CB under non-faulty conditions. The test is stopped after 4000 ms or when the CB closed due to nuisance tripping. Consequently, tests exhibiting response times in the order of 4000 ms are considered successful energisations, whereas those with significantly shorter response times are classified as failures of the normal energisation procedure.

The response types to non-faulty conditions for each test case are illustrated in Figure 38.

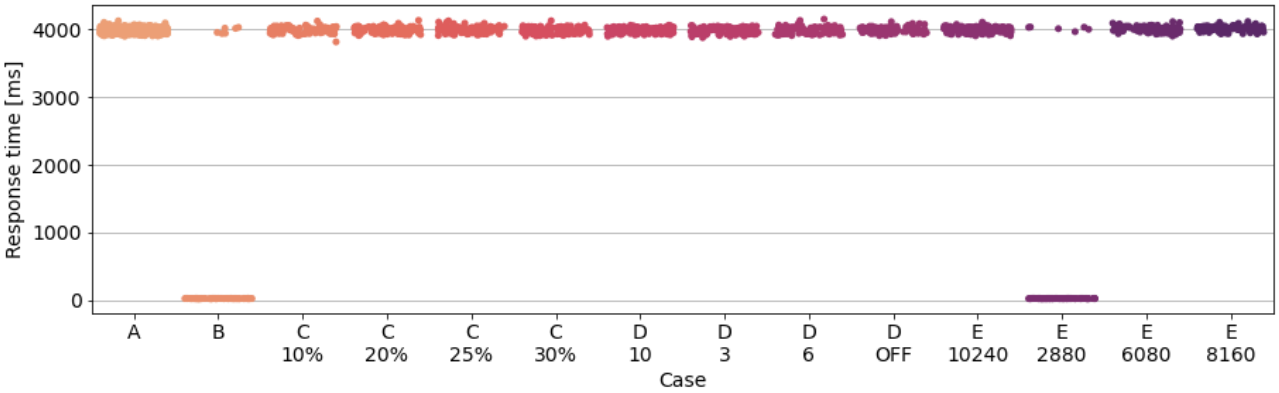

Figure 38: Spread of relay response times under non-faulty circumstances.

Nearly all variations of the relay configuration successfully energised under non-faulty conditions. A desirable result would have no premature tripping. However, two test cases did not. Test case B and the lowest value of Test case E did not show the desired reaction.

For Test case B, the inability to energise during non-faulty conditions stems from an improperly configured setting, namely Setting 2301. Setting 2301 determines whether the relay should restrain if the 2nd harmonic threshold is exceeded. The parameter is set to OFF in the configuration, meaning the relay will never restrain during energisation moments with high enough differential currents.

Changing Setting 1235 to 2880 A, such as in Test case E, prevents the network segment from properly energising. Therefore, Setting 1235 should not be configured too low, as this causes the relay to become overly sensitive. Therefore, a boundary exists between 2880 A and 6080 A beyond which the relay begins to trip under non-faulty conditions.

8.2.3 Summary of test cases

The results can be summarised into a comprehensive table. The best results per test case are the only relevant results, as only one value per setting can be used as the final recommendation. For example, if the setting value X results in a 20% malfunction rate while the setting value Y eliminates the malfunction, then the value Y would be the preferred choice. The summary of non-faulty and faulty energisations for all test cases is presented in Table 7.

Table 7: Summarisation of the results of the different relay parameters test cases under the original fault circumstances.

Test	Setting	Name	Trip-type during fault	Trips during energisation
A	-	Downloaded configuration	No trip	No
B	-	Setting statement	Trip	Yes
C	2302	2nd harmonic threshold	Trip	No
D	2310	Crossblock period	No trip	No
E	1235	I-DIFF>>switch threshold	Trip	No

In this table, the most desirable result would be a 'Trip' during fault and a 'No' under trips during energisation. The downloaded configuration Test case A responded as expected by replicating the malfunction. However, the other test cases produced unexpected or noteworthy results; these are listed below.

- Test case B **setting statement**: trips during energisation.
- Test case C **2nd harmonic threshold**: Performs as desired.
- Test case D **Crossblock period**: does not affect the relay's reaction during faults.
- Test case E **I-DIFF>>switch threshold**: Performs as desired.

Two parameter values are selected from the test cases for further testing, namely 20% for setting 2302 and 6080 A for setting 1235. Both new values for the settings show adequate behaviour for faulty and non-faulty conditions.

8.3 Testing for other fault circumstances

After the tests with the original circumstances were performed, two tests produced the desired results, namely Test case C and Test case E. The objective of the next tests is to see whether the proposed configuration performs as desired under different circumstances. Additionally, Test case A is simulated for all circumstances. This experiment acts as a baseline for comparison with the other test cases.

Test case A: downloaded configuration

For this experiment, each combination of the described fault circumstances is applied to the configuration of Test case A. The response times for each performed simulation can be seen in Figure 39.

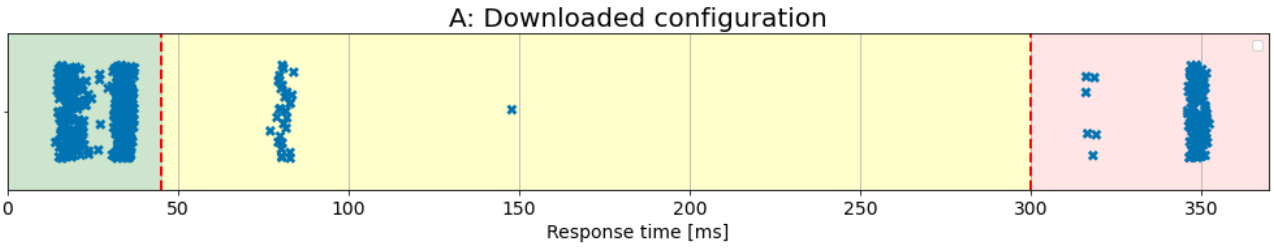

Figure 39: Spread of relay response time for Test case A for all circumstances.

In the Figure, a varied spread of response times can be seen. As expected, the malfunction persists under other fault circumstances. Additionally, the 'delayed trip' response type now also occurs, indicating that the different circumstances affect the functioning of the relay. The result of this experiment acts as a baseline for the other test cases.

Test case C: 2nd harmonic threshold

Setting 2302 was tested under the described circumstances. The response times when configuring the second harmonic threshold to 20% are plotted in Figure 40.

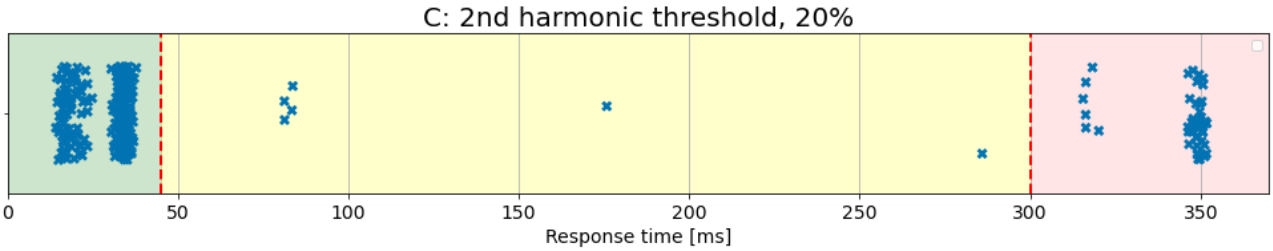

Figure 40: Spread of relay response time grouped for Test case C: 20% for all circumstances.

The setting that previously prevented the malfunction no longer does so when the relay is exposed to other combinations of fault circumstances. Comparing the results of this test case with Test Case A shows that it prevents the malfunction under some circumstances, but not all.

During the stage of testing with the original circumstances, configuring Setting 2302 to 25% and 30% had also provided desired results. Experiments with these values are introduced to conclusively eliminate setting 2302 as a viable solution. The response times of Test case C with 25% and 30% to all circumstances can be seen in Figures 41 and 42, respectively.

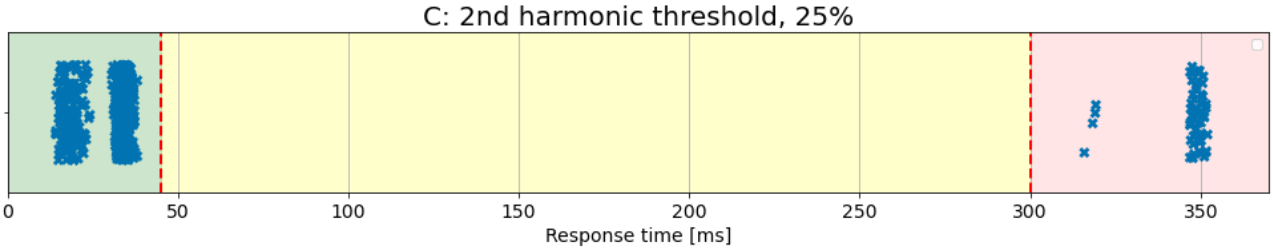

Figure 41: Spread of relay response time grouped for Test case C: 25% for all circumstances.

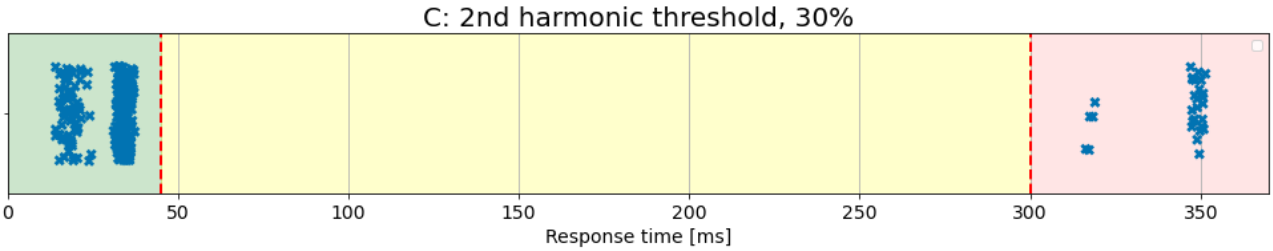

Figure 42: Spread of relay response time grouped for Test case C: 30% for all circumstances.

The results of testing with the setting configured to 25% and 30% reveals that the 'delayed trip' response type is prevented. However, the 'no trip' response type still remains. Due to the persistence of the malfunction, the experiments eliminate Setting 2302 as a viable solution.

Test case E: I-DIFF>>switch threshold

The different circumstances were applied to Setting 1235 to test its effectiveness and robustness in counteracting the malfunction. The response times when configuring the setting to 6080 A are plotted in Figure 43.

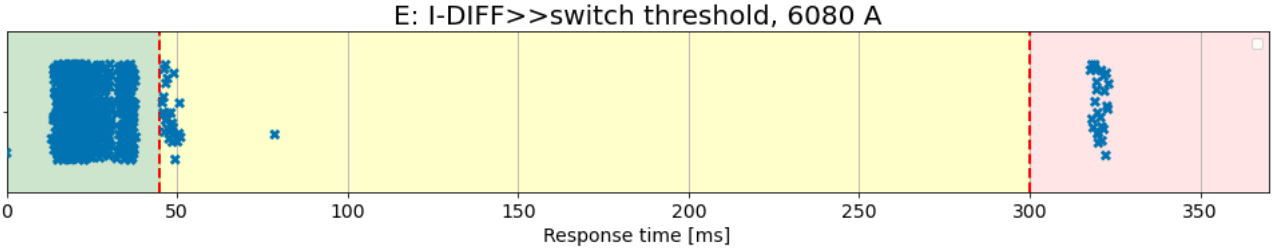

Figure 43: Spread of relay response time grouped for Test case E: 6080 A for all circumstances.

Figure 43 shows that the proposed setting change results in undesirable results. The 'no trip' malfunction persists under some circumstances. Moreover, several 'delayed trip' responses are recorded.

Testing with the original circumstances indicated that there exists a boundary where the protection scheme fails due to nuisance tripping. However, this boundary had not been explored. Therefore, another experiment

is introduced to conclusively eliminate setting 1235 as a viable solution. Test case E is repeated for all circumstances with Setting 1235 set to a lower value of 3500 A. The response times for this experiment are shown in Figure 44.

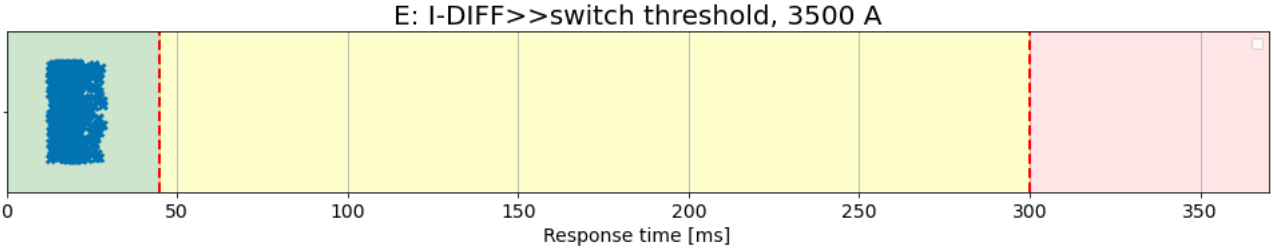

Figure 44: Spread of relay response time grouped for Test case E: 3500 A for all circumstances.

Figure 44 reveals that configuring Setting 1235 to 3500 A successfully prevents the malfunction from occurring under any combination of circumstances.

8.3.1 Susceptible fault circumstances

After the test cases were repeated for the described circumstances, it was found that other locations, scenarios, and conditions are also susceptible to the malfunction; some were more susceptible than the original circumstances. However, this statement does not apply to all variations. In some cases, the protection scheme still functioned correctly, indicating that the risk of malfunction depends on specific system configurations. This suggests that an analysis of the circumstances is needed.

The analysis will be performed by combining all the test results into one dataset. Afterwards, the data set is divided several times into different sets based on one of the circumstances: locations, scenarios, and conditions. These sets are then visualised to understand the influence of each circumstance.

Locations

Figure 45 shows the response times of all performed tests grouped by location. Location 6 was purposely omitted from the test because its results consistently exceeded 4000 ms, which would skew the data.

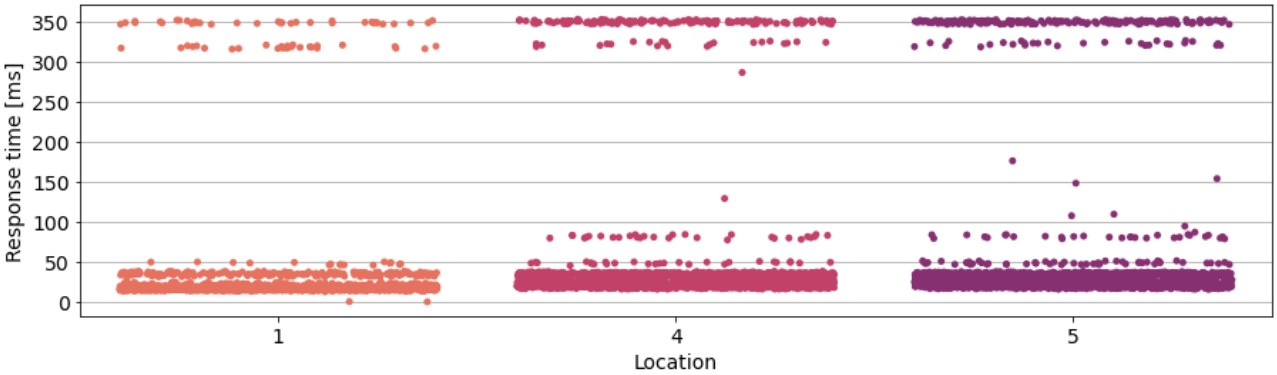

Figure 45: Spread of relay response time grouped by location.

It can be seen that the malfunction is present at any location. However, delayed responses become more likely the higher the impedance of the affected grid segment. Moreover, location 4 and 5 have a higher number of malfunctions compared to location 1. The further away from the open CB, the lower the fault current, the more likely the relay is to malfunction.

Scenarios

Figure 46 shows the response times of all performed tests grouped by scenario.

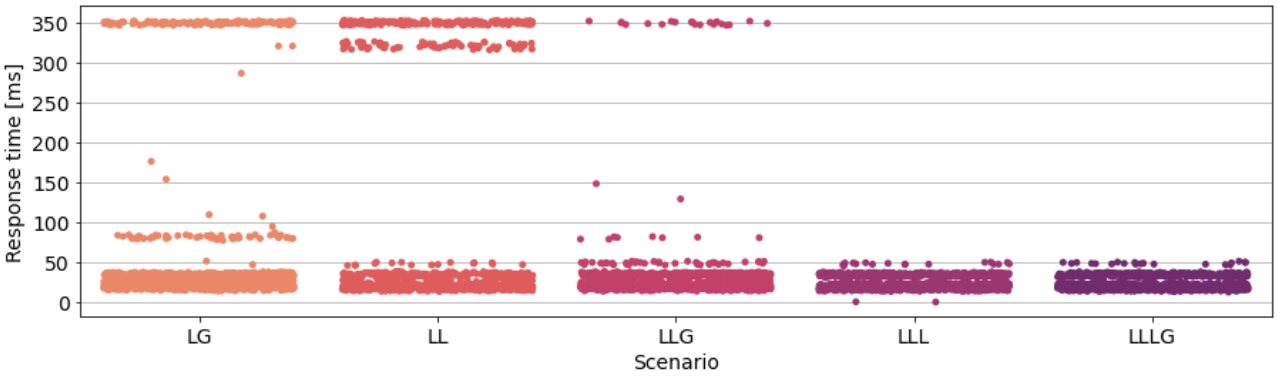

Figure 46: Spread of relay response time grouped by scenario.

The type of scenario has a substantial effect on the malfunction. The malfunction occurs under three scenarios: a LG fault, a LL fault, and a LLG fault. More specifically, the grounded faults (i.e. LG and LLG) display 'delayed trip' responses, whilst the 'no trip' response is the only type that occurs during a LL fault.

Conditions

Lastly, the dataset is divided into condition-based sets. The response time for each condition can be seen in Figure 47.

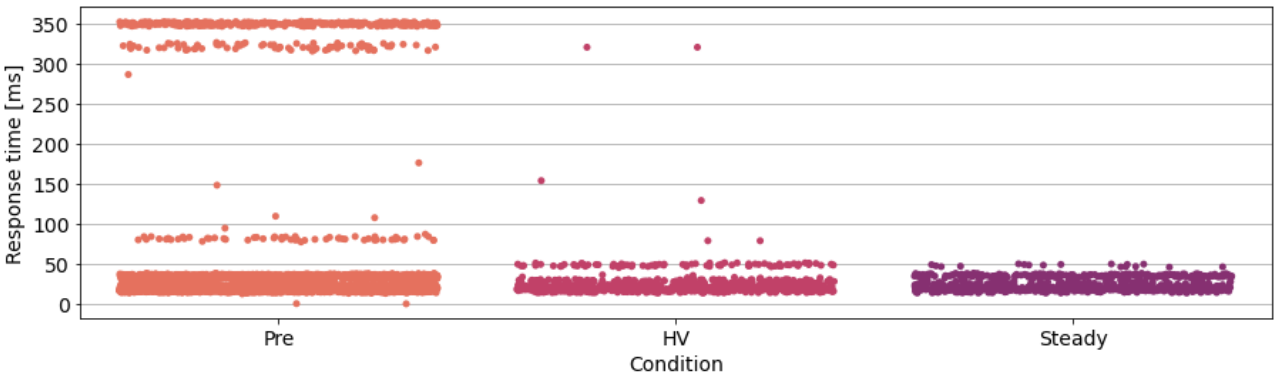

Figure 47: Spread of relay response time grouped by condition.

It can be seen that pre-energisation faults are the only condition in which the malfunction occurs, except for a small number of outliers. This supports the conclusion that the 'under switch-on condition' settings are the root cause of the issue, as the condition primarily influences this aspect of relay behaviour.

There are several exceptions for the HV side energisation condition, which show a delayed reaction. However, these are assumed to be faults in the simulation, rather than the relay operations. When testing, simulated faults were rapidly induced. The rapid succession of faults causes remanent flux to build in the transformer's and CTs' cores, which causes the simulation to operate unpredictably.

8.4 Analysis of the combined test results

Several conclusions can be made based on the results from the experiments. This section presents the results of the test cases and assesses whether each setting should be recommended for change.

8.4.1 Non-configurable parameters

Many non-configurable relay parameters were uncovered during this research and testing. For example, setting 2302 did not prevent the malfunction. Configuring a setting might induce undesirable consequences. This section aims to give a list of non-configurable parameters and explore the consequences of altering the settings.

2301: Inrush Restraint

Magnitizing inrush current is expected during the energisation of a network segment with a transformer. A reliable method of preventing nuisance tripping due to inrush current is through harmonic inrush restraint. Therefore, it is not recommended to disable the inrush restraint function through Setting 2301 to 'OFF'.

2302: 2nd harmonic in % of fundamental

Traditionally, the restraint threshold for harmonic inrush restraint is set to 15% to 20%. Raising the threshold value will decrease the sensitivity of the restraining function. The loss of sensitivity is specifically of interest during non-faulty energisations. If the second harmonic threshold is set too high, differential protection schemes may fail to activate the harmonic inrush restraint function, increasing the risk of nuisance tripping.

Furthermore, the conclusion drawn from the results of Test case C is that adjusting Setting 2302 would not prevent the malfunction in all circumstances. Therefore, increasing the second harmonic threshold of the inrush restraint function through Setting 2302 is not a recommended method of preventing the malfunction.

8.4.2 Suggested parameters for adjustment

A final suggestion needs to be made to prevent the malfunction in the future for all grid segments that have the discussed protection devices implemented. This chapter has built up to this conclusion, trying to make a final recommendation that is as robust as possible.

2310: Crossblock period

The results of Test case D show that Setting 2310 does not affect the response type of the relay to faults. The crossblock function seems not to operate as intended or have any effect during this specific fault. It is not recommended to adjust the crossblock period setting to prevent the malfunction.

On the other hand, it would be favourable to select a better time than the currently selected value of the downloaded configuration, which is an infinite delay. The value specified in the setting statement (i.e. 30 ms) is likely to yield better results in scenarios where the crossblock functionality is beneficial, such as during ultra deep saturation of the transformer [24]. Therefore, it is recommended to adapt Setting 2310 to a suitable value.

1235: I-DIFF>> Value under switch on condition

The result of Test case E reveals that Setting 1235 offers a viable solution to prevent the malfunction. By lowering the setting to the value of 3500 A, the network segment can still be energised, and the I-Diff>> can capture faults of similar magnitudes.

The recommended value by Siemens for Setting 1235 is three to four times the rated current of the circuitry [3], which is approximately 3884 A. The assigned value is 12250 A. The discrepancy between the two values is the cause of the malfunction; the value assigned to Setting 1235 in the downloaded configuration decreases the sensitivity of the relay too much.

It is recommended to adjust Setting 1235 to a more suitable value, such as 3500 A, to prevent maloperations in the future. A new value for Setting 1235 should still allow the grid segment to energise without nuisance tripping and prevent high magnitude faults with the I-Diff>> function.

9 Conclusion

The main purpose of this report was to provide recommendations for preventing delayed response times caused by transformer inrush-induced harmonic content by adjusting the implemented relay configurations. For this purpose, a case study using the RTDS was performed to investigate the effect of altering relay settings on the malfunction.

The test cases that were simulated identified two settings that should not be configured and two that should be adjusted for more optimal relay operations. Interestingly, whilst the malfunction only occurs during faults with significant second harmonic content, the solution is not directly related to the harmonic inrush restraint function. The experiments identified that the I-Diff>> function was improperly configured. Specifically, the switch-on condition threshold of the functionality (i.e. Setting 1235) was set too high, which made the function insensitive to faults in the network.

Adjusting the setting to a suitable value completely prevented the malfunction, not only for the presented fault but also for all relevant fault circumstances simulated in the protected region using the RTDS. This provided a robust and effective solution to counteract the malfunction. The solution found using the test cases allows protection engineers to identify other protected regions that might be susceptible to the malfunction. Similar protection schemes can be checked and adjusted if the same problem is detected.

The I-Diff>> function of the Siprotec 4 7SD5 is a powerful tool that should allow quick disconnection during high magnitude faults. However, the calculation of differential current through charge comparison should be configured to be sensitive to faults. Otherwise, the relay will exhibit unintended behaviour and be susceptible to malfunctions.

10 Future Work

Due to the limited scope and time constraints, other interesting topics were left out of this project, which might be relevant to explore. This includes different types of relays in the HIL setup or a deeper investigation of the crossblock functionality of the Siprotec 4 7SD5.

10.1 Different relay types in the Hardware-in-the-Loop setup

Besides the type of relay discussed in the thesis (Siemens Siprotec 4 6SD5), two more relay models are of interest: the Siemens Siprotec 5 7SL8 and the GE MiCOM p545. The currently installed relay is outdated and will no longer be implemented. The other relays will serve as replacements. Therefore, it is beneficial to study the effect of this network configuration on the newer models. The relevant relays are shown in Figure 48.

(a) Siemens Siprotec 4 7SD5 (b) Siemens Siprotec 5 7SL8 (c) General Electric MiCOM p545

Figure 48: Overview of all Relay models.

10.2 Investigation of the crossblock function

Test case D revealed that the crossblock did not affect the response type. However, in the event log, it could be seen that the harmonic inrush restraint module blocked all phases, whilst the second harmonic threshold was not reached in all phases. Therefore, the crossblock function operated but was unaffected by altering crossblock-specific settings, such as Setting 2310.

It would be an interesting investigation to see the effect of the crossblock function. It is beneficial to solve questions such as: Does the crossblock function work as intended? Are there other situations where the crossblock function shows the same behaviour?

Siprotec 4 7SD5 Settings

Setting	Description	Page
0251	k_alf/k_alf nominal	13–15
0253	CT error in % at k_alf/k_alf nominal	13–15
0254	CT error in % at k_alf nominal	13–15
1210	I-DIFF >: Pickup value	13–15, 27, 30
1213	I-DIFF >: Value under switch on condition	13–15, 27, 30, 31
1233	I-DIFF >>: Pickup value	15, 27, 28, 30
1235	I-DIFF >>: Value under switch on condition	15, 26–28, 30, 31, 35–38, 40, 41
2301	Inrush Restraint	15, 27, 28, 35, 40
2302	2nd harmonic in % of fundamental	15, 26–28, 33–37, 40
2305	Maximum inrush-peak value	15, 27
2310	Time for Crossblock with 2nd harmonic	15, 26–28, 34, 35, 40, 42

Acronyms

Acronym	Definition	Page
ALF	Accuracy Limit Factor	13–15
CB	Circuit Breaker	5, 7, 10, 11, 14–17, 20, 23–25, 29–31, 35, 38
CT	Current Transformer	5–7, 10–14, 18, 20, 24, 39
D/A	Digital-to-Analogue	17
EHM110	Eemshaven Midden 110 kV	2, 29
GTAO	Gigabit-Transceiver Analogue Output	16–18, 22
GTFPI	Gigabit-Transceiver Front Panel Interface	16, 17
HIL	Hardware-in-the-Loop	ii, 3, 16, 17, 25, 26, 42
HV	High-Voltage	4–6, 13, 17, 18, 25, 26, 29, 30, 39
LG	Single-phase to Ground	4, 21, 22, 26, 29, 30, 39
LL	Phase-to-Phase	21, 29, 30, 39
LLG	Phase-to-Phase to Ground	21, 29, 30, 39
LLL	Three-Phase	21, 29, 30
LLLG	Three-Phase to Ground	21, 29, 30
LV	Low-Voltage	5, 6, 17, 18, 21, 25, 29, 30
MV	Medium-Voltage	5
RBB220	Robbenplaat 220 kV	2, 4, 29
RTDS	Real Time Digital Simulator	ii, 1, 2, 16–18, 20, 22, 29, 41
TSO	Transmission System Operator	1
UHV	Ultra-High-Voltage	5

References

[1] TenneT, "Incident and Outage Report." Internal report, Dec. 2021. Confidential internal document. Used and documented by TenneT.

[2] TenneT, "Incident Reports Summary." Internal report, Dec. 2021. Confidential internal document. Used and documented by TenneT. Contains 12 hour, 24 hour and 5 day analysis.

[3] SIEMENS, "SIPROTEC 4 Line Differential Protection with Distance Protection 7SD5 Manual," 05 2016. Device Manual.

[4] Prysmian, "Rapportage Onsite Beproevingen, Trafo 211-2 EHM - OS Robbenplaat." Internal documentation, Prysmian Group, 03 2020. Order No. 1526000695, Used internally at TenneT; not publicly available.

[5] SIEMENS, "Transformer Test Report." Internal documentation, SIEMENS, 01 2019. Used internally at TenneT; not publicly available.

[6] Pfiffner, "Transformerpass 110720 Index 00, Outdoor Combined Transformer Um = 245 kV." Internal documentation, Pfiffner, 04 2015. Used internally at TenneT; not publicly available.

[7] Pfiffner, "SF6-Combined Transformer Routine test report." Internal documentation, Pfiffner, 01 2019. Used internally at TenneT; not publicly available.

[8] TenneT, "Beveiliging instelverklaring, Station: Robbenplaat 220 kV RBB220." Internal documentation, TenneT, 2019. Internal document, not publicly available.

[9] A. Sultan, M. Mustafa, and M. Saini, "Ground fault currents in unit generator-transformer at various ngr and transformer configurations," in *2012 IEEE Symposium on Industrial Electronics and Applications*, pp. 136–140, 2012.

[10] B. Kasztenny, M. Thompson, and D. Taylor, "Time-domain elements optimize the security and performance of transformer protection," 03 2018.

[11] C. Bayliss and B. Hardy, "Chapter 10 - relay protection," in *Transmission and Distribution Electrical Engineering (Fourth Edition)* (C. Bayliss and B. Hardy, eds.), pp. 287–359, Oxford: Newnes, fourth edition ed., 2012.

[12] S. Saad, A. Elhaffar, and K. El-Arroudi, "Optimizing differential protection settings for power transformers," 07 2015.

[13] R. Hunt, J. Schaefer, and B. Bentert, "Practical experience in setting transformer differential inrush restraint," in *2008 61st Annual Conference for Protective Relay Engineers*, pp. 118–141, 2008.

[14] H. Bronzeado, S. Pinto, P. Jonsson, J. Oliveira, and M. L. Chaves, "Controlled energizing of three-phase transformer: Analysis of test results," 01 2007.

[15] N. Chen, C. Wang, J. Zhang, F. Yang, Y. Chen, and W. Hong, "The inrush current analysis and restraining method of energizing no-load transformer," p. 204 – 207, 2017.

[16] A. Guzman, S. Zockoll, G.Benmouyal, and H. Altuve., "Performance analysis of traditional and improved transformer differential protective relays," *36th Annual Minnesota Power Systems Conference*, 11 2000.

[17] T. C. Monteiro, F. O. Martinz, L. Matakas, and W. Komatsu, "Transformer operation at deep saturation: Model and parameter determination," *IEEE Transactions on Industry Applications*, vol. 48, no. 3, pp. 1054–1063, 2012.

[18] Siemens, "Engineering software for SIPROTEC 4 and SIPROTEC Compact – DIGSI 4 – Siemens AG — siemens.com." https://www.siemens.com/global/en/products/energy/energy-automation-and-smart-grid/protection-relays-and-control/engineering-tools-for-protection/engineering-software-digsi-4.html. [Accessed 07-07-2025].

[19] RTDS, "Graphical User Interface." https://www.rtds.com/technology/graphical-user-interface, 2025. [Accessed 07-07-2025].

[20] C. L. Fortescue, "Method of symmetrical co-ordinates applied to the solution of polyphase networks," *Transactions of the American Institute of Electrical Engineers*, vol. 37, no. Part II, pp. 1027–1140, 1918. Presented at the 34th Annual Convention of the AIEE, Atlantic City, NJ, 28 June 1918.

[21] J. L. Blackburn, *Symmetrical Components for Power Engineering.* Boca Raton, Florida: CRC Press, 1993.

[22] Y. Liang, Y. Zhang, and A. Dehkordi, "Key Aspects in Modelling Transformers for Real Time Simulation: Open Phase, DC Bias and Internal Faults," in *2019 IEEE 8th International Conference on Advanced Power System Automation and Protection (APAP)*, (Xi'an, China), pp. 1891–1895, IEEE, 2019.

[23] Y. Zhang, T. Maguire, and P. Forsyth, "UMEC Transformer Model for the Real Time Digital Simulator," in *Proceedings of the International Conference on Power Systems Transients (IPST)*, (Montreal, Canada). Paper No. IPST05-077-25a.

[24] S. Hodder, B. Kasztenny, N. Fischer, and Y. Xia, "Low second-harmonic content in transformer inrush currents - analysis and practical solutions for protection security," pp. 705–722, 03 2014.

[25] R. Nisticò, F. Cesano, and F. Garello, "Magnetic materials and systems: Domain structure visualization and other characterization techniques for the application in the materials science and biomedicine," *Inorganics*, vol. 8, no. 1, 2020.

A Additional Differential Protection Background

Additional information on the underlying natural phenomena of differential protection is provided in this section. This section explains the key component of harmonic content, which is transformer core saturation. Moreover, an example where crossblock is required is given. Finally, the mechanics behind capacitive inrush is also addressed.

A.1 Saturation in the transformer core

Saturation can be understood by explaining magnetic domains and magnetic moments with and without an external magnetic field, and by examining a graph plotting the flux field density B versus the magnetising force H (i.e., the BH characteristic curve of a transformer core). These images are seen in Figures 49a, 49b and 49c, respectively.

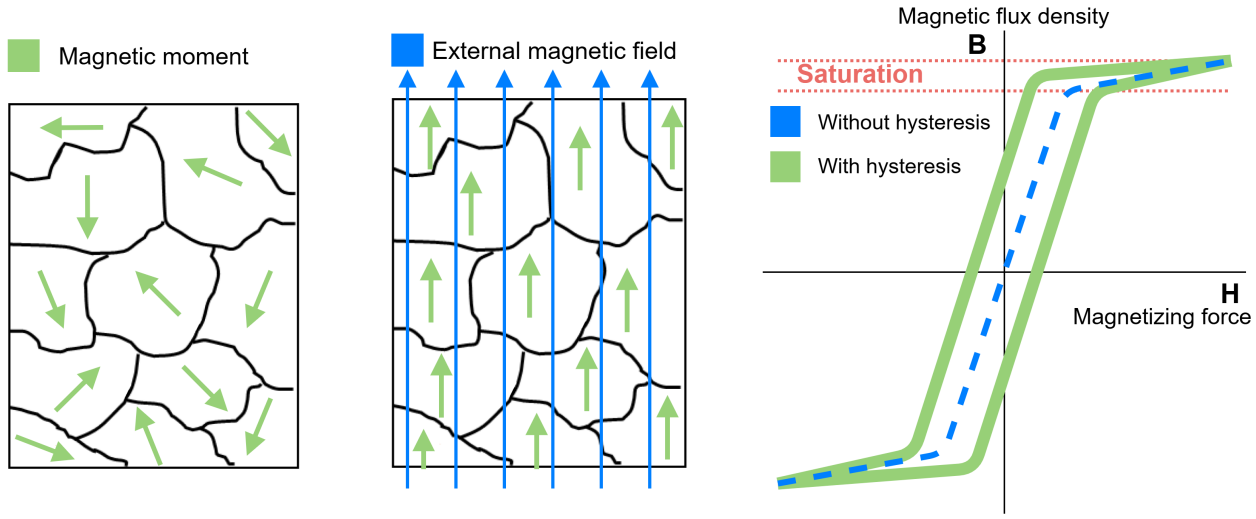

(a) Random alignment of magnetic moments [25].

(b) Alignment due to external magnetic field [25].

(c) Arbitrary BH-curve.

Figure 49: Representation of a microscopic zoom in on an arbitrary magnetic material along with a BH-curve.

Figures 49a and 49b show a microscopic zoom-in representation of the material of a transformer core, which is typically electric steel. The material is divided into smaller segments, called magnetic domains, and each domain possesses its own magnetic moment.

Before any energisation, each magnetic moment has an arbitrary orientation. An external magnetic field will be created when an excitation voltage is applied to the transformer's windings. When this magnetic field is used to align magnetic domains, an empirical process of aligning the magnetic moments with the field will start. The core is *saturated* when all the magnetic moments are aligned.

The effects of saturation can be observed in the BH curve [24], as shown in Figure 49c. In the middle, a slight increase in flux equals a small increase in magnetising force. In the outer ends, when the core saturates, the same increase in flux equals a tremendous increase in magnetising force.

Additionally, the permeability of a material $\mu_0\mu_r$ can be derived from the BH-curve by dividing B by H. Normally, the relative permeability of electrical steel, a frequently used core material, can be in the range of 2.000 to 38.000. However, as the core approaches saturation, the relative permeability will decrease to 1; the transformer core will be as effective as a vacuum.

Figure 50 shows an equivalent circuit model of a transformer.

Three parameters in this model stand out: the input voltage V_1, the excitation voltage E_1 and the magnetising inductance L_M. The excitation voltage can be seen as a voltage division of the input voltage between two impedances, $R_1 + X_{l1}$ and $G_C||L_M$. The formula for the magnetising inductance is given in Equation 9.

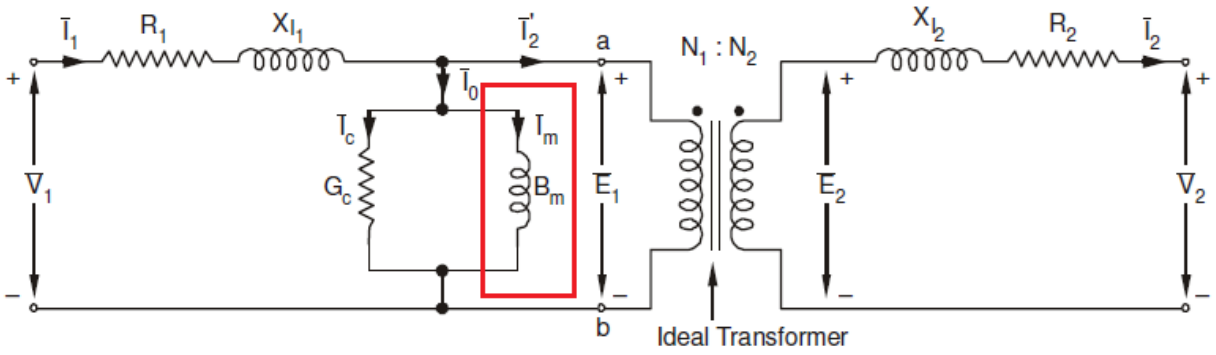

Figure 50: Equivalent circuit model of a transformer.

$$L_M = \frac{N^2 \cdot A_C \cdot \mu_0 \cdot \mu_r}{l} \tag{9}$$

In this equation, L_M is the transformer's magnetizing inductance $[H]$, N is the number of winding turns [-], A_C is the cross sectional area of the core $[m^2]$, μ_0 is the absolute permeability of the core $[H/m]$, μ_r is the relative permeability of the core [-], and l is the length of the core $[m]$.

Evidently, when the relative permeability μ_r drops, the excitation voltage will also drop. Thus, a high current will be drawn throughout the transformer's primary windings and not be transferred to the secondary side. This means a differential current will flow called *magnetising inrush current*.

A.2 Balanced flux within the transformer core

Under normal operating conditions, a power system is balanced across its three phases. For example, when one phase conducts a large amount of current, the other two phases act as the return path for that current. It is also possible for a phase to have a low instantaneous current. This is also true for core flux density and magnetising inrush currents. This concept can be seen in Figure 51.

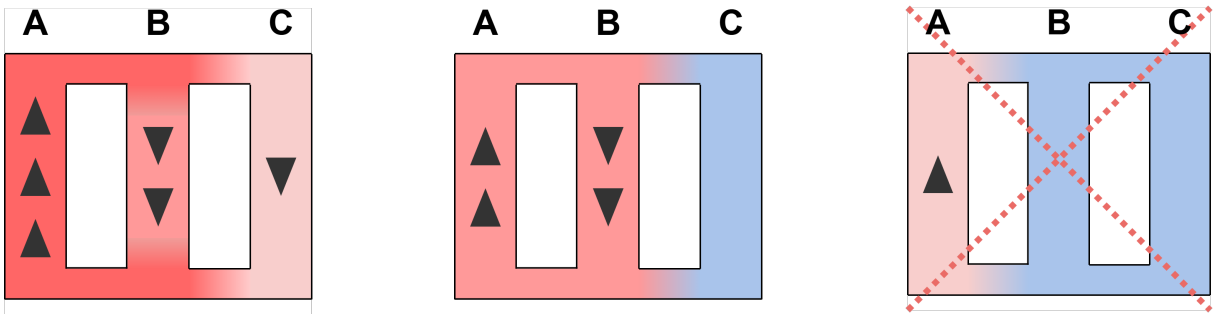

(a) Flux balanced over all phases (b) Flux balanced between 2 phases (c) Impossible imbalance

Figure 51: Demonstration of the balance of flux accross the limbs of a transformer.

Magnetic flux lines always form a closed loop. The sum of the flux passing through each winding must be zero at any given time, given that the leakage flux is negligible.

It is evident that some phases may experience overflux and saturation while others do not. This becomes particularly problematic in cases of ultra-deep saturation, where a deeply saturated phase generates inrush current without producing harmonic content [17], which would not engage the inrush restraint functionality. This outcome underscores the necessity of implementing crossblock.

A.3 Cable capacitive inrush current

Any transmission line is electrically linked to the ground and the other phases. The linkage capacitance is based on the parameters of the line, including the dielectric material, conductor size, and number of strands. A model

of a transmission line is the lumped element model, as seen in Figure 52.

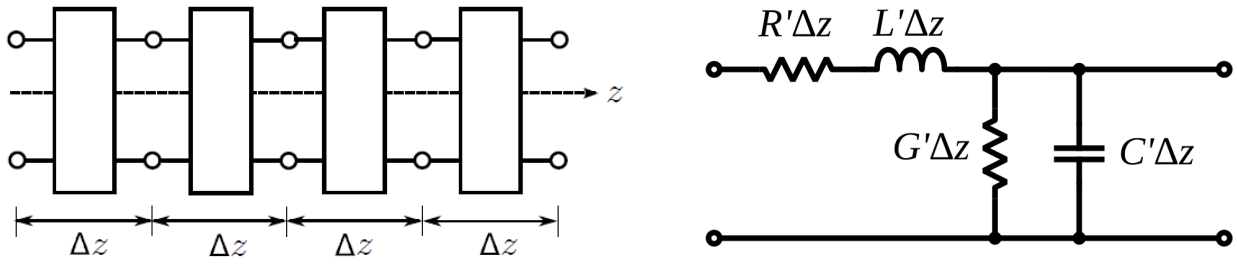

(a) The cable is divided into small fragments with length Δz (b) Each fragment is made up of 4 lumped components.

Figure 52: Lumped element model of a transmission line

The lumped element model contains four variables: the combined per unit length resistance R' $[\Omega/m]$, the leakage-current per unit length conductance G' $[S/m]$, the per unit length inductance L' $[H/m]$ and the per unit length capacitance C' $[F/m]$.

Before energising, no energy is stored in the electric field of the capacitive elements. Closing a circuit breaker can be viewed as applying an impulse voltage source to the input of the lumped model. Impulse waveforms mainly consist of high-frequency harmonics. A capacitor acts as a short circuit when a high-frequency signal is applied to it. Therefore, a high and fast inrush current will be generated.

B Most fault-prone circumstances

It can be concluded that some faults are more susceptible to malfunction. The only relevant system condition is the pre-energisation fault. However, which location and scenario are the most prone to the discussed erroneous behaviour?

To find which location and scenario are the most fault-prone, Figure 53 shows the response times of all performed tests grouped by location and scenario.

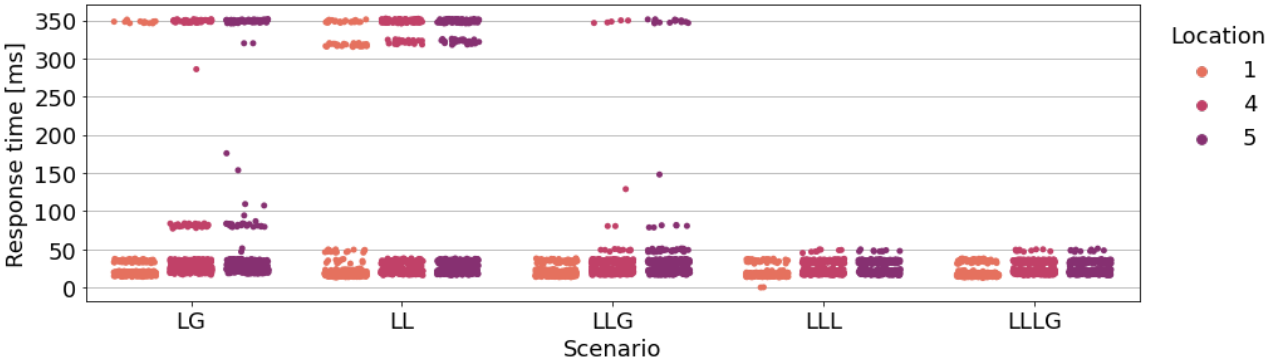

Figure 53: Spread of relay response time grouped by scenario and location.

The following two pages plot the response times for all test cases. Figure 54 show the response times of the test cases with the original test cases, and Figure 55 show the response times of the test cases with all circumstances.

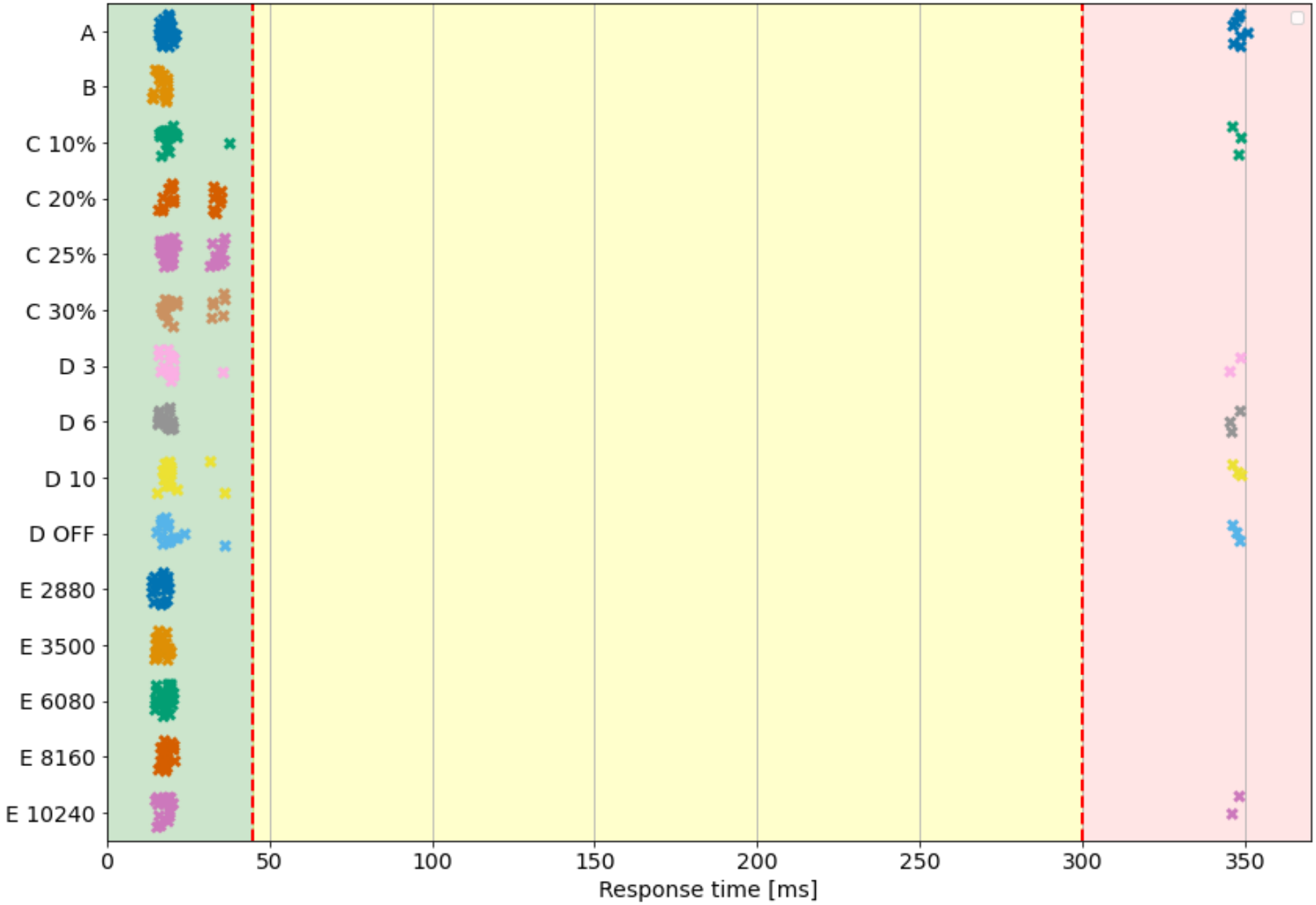

Figure 54: Spread of relay response time grouped by all test cases with the original test circumstances.

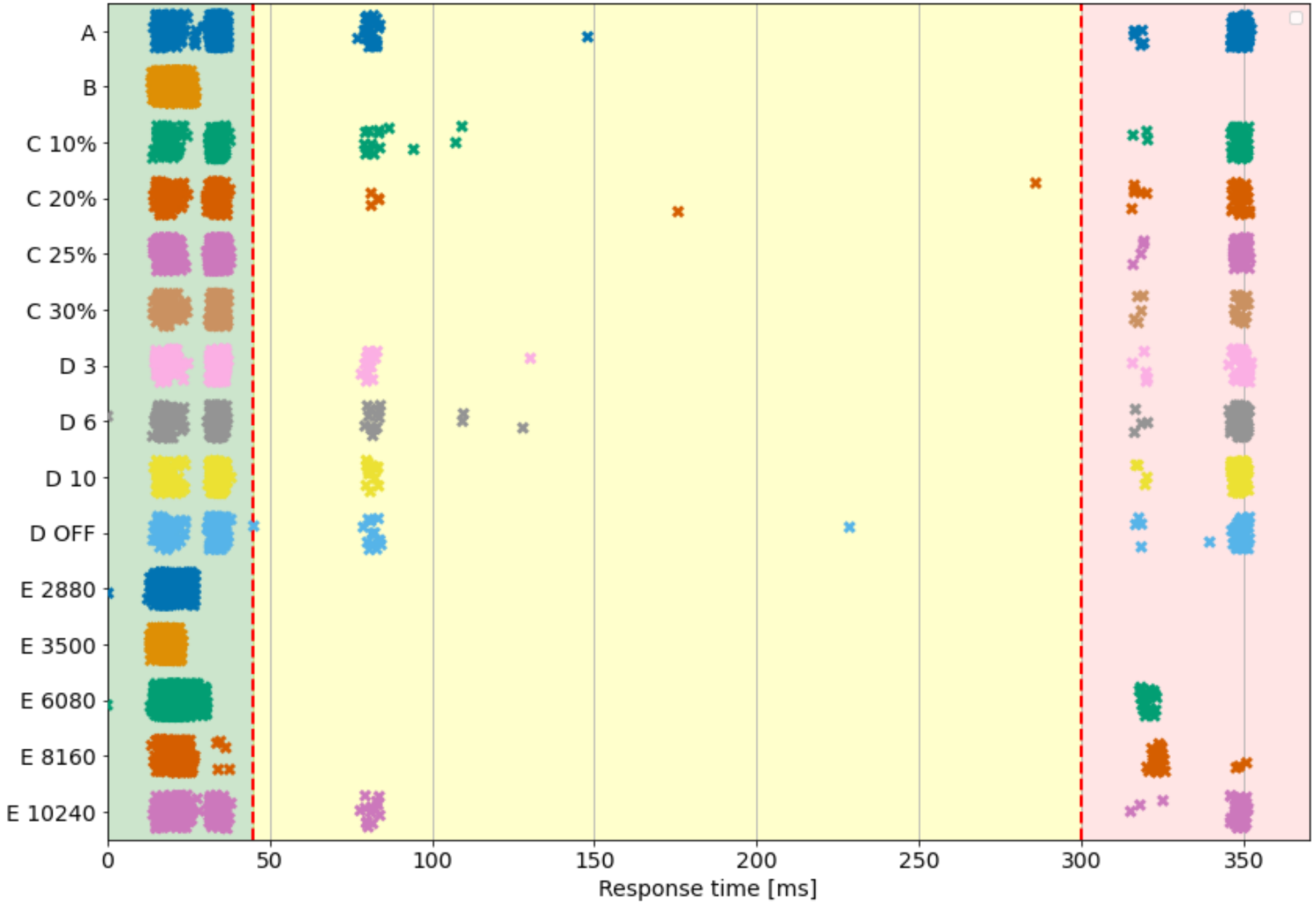

Figure 55: Spread of relay response time grouped by all test cases for all circumstances.